Motor context dominates output from Purkinje cell functional regions during reflexive visuomotor behaviours

Laura D. Knogler, Andreas M. Kist, Ruben Portugues*

Max Planck Institute of Neurobiology, Sensorimotor Control Research Group, Martinsried, Germany

*For correspondence: rportugues@neuro.mpg.de

SUMMARY

The cerebellum integrates sensory stimuli and motor actions to enable smooth coordination and motor learning. We use population imaging and single-cell electrophysiology while monitoring behavior to find the neural correlates of sensory and motor variables in the cerebellar Purkinje cell population during visually-driven behaviors in larval zebrafish. We find that Purkinje cells functionally cluster into three regions that receive similarly tuned, sensory climbing fiber input relating to distinct visual features. In contrast, the simple spike output of nearly all Purkinje cells is strongly driven by motor-related tail and eye signals. At rest, complex spikes modulate simple spike rates over hundreds of milliseconds in a cell-specific way, whereas during swimming, complex spikes have a very acute temporal effect on already high simple spike rates. Our findings highlight the importance of motor context for cerebellar computations and provide the first comprehensive description of sensorimotor coding across the Purkinje cell population during behavior.

INTRODUCTION

Decades of influential anatomical (Eccles et al., 1967; Palay & Chan-Palay, 1974), theoretical (Marr, 1969; Albus, 1971; Ito, 1972) and experimental work (see Ito, 2006 for a review) have led to our current knowledge highlighting the cerebellum as a major brain region for the control of motor behaviors. The ability of the cerebellum to guide motor control and learning relies critically on the integration of sensory and motor-related signals in Purkinje cells, as these neurons constitute the main computational units and output of the cerebellum.

The anatomy and physiology of Purkinje cells across vertebrates displays several distinctive features that are thought to underlie an important functional role in the cerebellum. Purkinje cells receive two excitatory input streams, via parallel fibers from granule cells and a single climbing fiber from the inferior olive, that differentially modulate their spike output. Across vertebrate species, climbing fibers from inferior olivary neurons drive complex spikes in Purkinje cells at a spontaneous rate of ~0.5-2 Hz whereas parallel fiber inputs modulate intrinsic simple spike activity at much higher rates (tens of Hz in larval zebrafish, Hsieh et al., 2015, and up to hundreds of Hz in mammals, Eccles et al., 1967; Raman & Bean, 1997). Simple spike output can furthermore be biased to burst or pause by the arrival of a complex spike (Mathews et al., 2012; Badura et al., 2013; Sengupta & Thirumalai, 2015), though the precise nature of this relationship varies across Purkinje cells (Zhou et al., 2014, 2015; Xiao et al., 2014). Although little is currently known about molecular layer interneurons in the zebrafish cerebellum (Bae et al., 2009), findings in mammalian cerebellum suggest that inhibitory interneurons may also exert considerable control over simple spike rates (Dizon & Khodakhah, 2011; ten Brinke et al., 2015; Jelitai et al., 2016).

Motor learning requires the coincident arrival of relevant sensorimotor information in the cerebellum along the climbing fiber and parallel fiber synapses to drive synaptic plasticity at parallel fiber to Purkinje cell synapses, among others (see Gao et al., 2012 for review). Sensory and motor information must therefore be consistently encoded in the cerebellum to provide the foundation for motor learning to take place. Nevertheless, there is little consensus regarding the population-wide organization of sensory and motor information to Purkinje cells via these different channels. Climbing fibers have been variously described as carrying sensory and/or motor signals (see Ito, 2013 for review), which may reflect regional differences in coding or an inability to disambiguate correlated sensorimotor signals during behavior. Furthermore, there is great debate about whether climbing fiber signals convey error, novelty, or predictive signals (see Simpson et al., 1996 and

Streng et al., 2018 for reviews). Granule cells were previously thought to convey mostly sensory context (see Arenz et al., 2009, for review) but have more recently been shown to robustly encode both current (Ozden et al., 2012; Powell et al., 2015; Knogler et al., 2017) and predicted behavioral state (Giovannucci et al., 2017) and even cognitive signals such as the expectation of reward (Wagner et al., 2017). In Purkinje cells, many studies have demonstrated that simple spiking driven by parallel fiber input can correlate with movement kinematics related to some aspect of behavior (see Popa et al., 2018 for areview). Nonetheless, it is challenging to interpret how individual Purkinje cells integrate both sensory and motor variables since mammalian Purkinje cells have particularly high spontaneous simple spike firing rates and are estimated to receive input from 100,000 - 200,000 parallel fibers (Harvey & Napper, 1991).

At the population level, Purkinje cells in the mammalian cerebellum are generally organized into four transverse zones along the rostrocaudal axis based on the anatomy of the climbing fiber projections (Ozol et al., 1999) and further subdivided into longitudinal zones and microzones defined by additional anatomical, physiological and molecular features (see Apps & Hawkes, 2009 for review). This organization is thought to produce functional modules that each participate in the control of a certain set of behaviors (Cerminara & Apps, 2011), however the precise link between Purkinje cell physiology and the behavioral relevance of cerebellar modules is not well understood. The large number of Purkinje cells in the mammalian cerebellum (estimated at >300,000 in the rat cerebellum; Harvey & Napper, 1991) precludes the ability to comprehensively monitor activity across the Purkinje cell layer to determine if the same computations are performed throughout the cerebellum.

In this study, we use larval zebrafish to study how sensorimotor variables are encoded in Purkinje cells and how these responses are functionally organized across the cerebellum with respect to the most important reflexive visuomotor behaviors performed by these animals. The larval zebrafish cerebellum is anatomically organized in a typical vertebrate tri-layered configuration, with a population of approximately 500 Purkinje cells, each receiving inputs from many parallel fibers and likely just one climbing fiber (Bae et al., 2009; Hashimoto & Hibi, 2012; Hsieh et al., 2014; Hamling et al., 2015). Several studies have demonstrated a functional role for the cerebellum in the larval zebrafish relating to motor coordination, adaptation, and learning (Aizenberg & Schuman, 2011; Ahrens et al., 2012; Matsui et al., 2014; Portugues et al., 2014; Harmon et al., 2017). We took advantage of the small size of the cerebellum in larval zebrafish and its accessibility for physiological recordings to perform functional mapping of Purkinje cell sensorimotor responses

across the entire population during spontaneous and visually-evoked reflexive swimming and eye movements (the optomotor and optokinetic response, respectively). These uncover a striking organization of the Purkinje cell population into three functional regions that receive similar motor-related parallel fiber input but are strongly differentiated by sensory complex spike responses relating to different visual features of reflexive visuomotor behaviors. These findings reveal the organization of cerebellar modules underlying innate behaviors and thus provide a foundation for future studies of motor learning in the cerebellum.

RESULTS

Activity in the cerebellum is arranged into functionally-defined and anatomically-clustered symmetrical regions of Purkinje cells

Anatomical, physiological, and genetic studies of the mammalian cerebellum across species show that the cerebellar cortex is organized into spatially-restricted functional regions of Purkinje cells, where a given region has a specific set of inputs and outputs and is thought to control the coordination and adaptation of a different set of sensorimotor behaviors (Apps & Hawkes, 2009; Witter & De Zeeuw, 2015). In order to describe the organization of Purkinje cells across the entire cerebellum for the first time, we performed population imaging across all Purkinje cells while driving reflexive sensorimotor behaviors. We presented a variety of visual stimuli to awake, head-embedded fish whose eyes and tail were freed and we observed consistent eye and tail movements in response to visual stimuli (Figure 1a; Easter & Nicola, 1996). These included whole-field gratings moving in the four cardinal directions that elicited reflexive optomotor swimming responses, and a windmill pattern centered on the larva's head rotating with a sinusoidal velocity that elicited a reflexive optokinetic response of the eyes to track the movement. Moving gratings evoked varying degrees of swimming behavior depending on the direction and speed in which they were presented, and whole-field flashes were included to provide stimuli that evoke very little behavior (Figure 1a). The visual stimuli were presented in open loop (e.g. with no updating of the visual stimuli in response to behavior) in order to clearly disambiguate sensory versus motor contributions to neural activity. We performed 2-photon functional imaging of the entire Purkinje cell population in response to this set of stimuli while tracking eye and tail movements (Figure 1b, Movie S1).

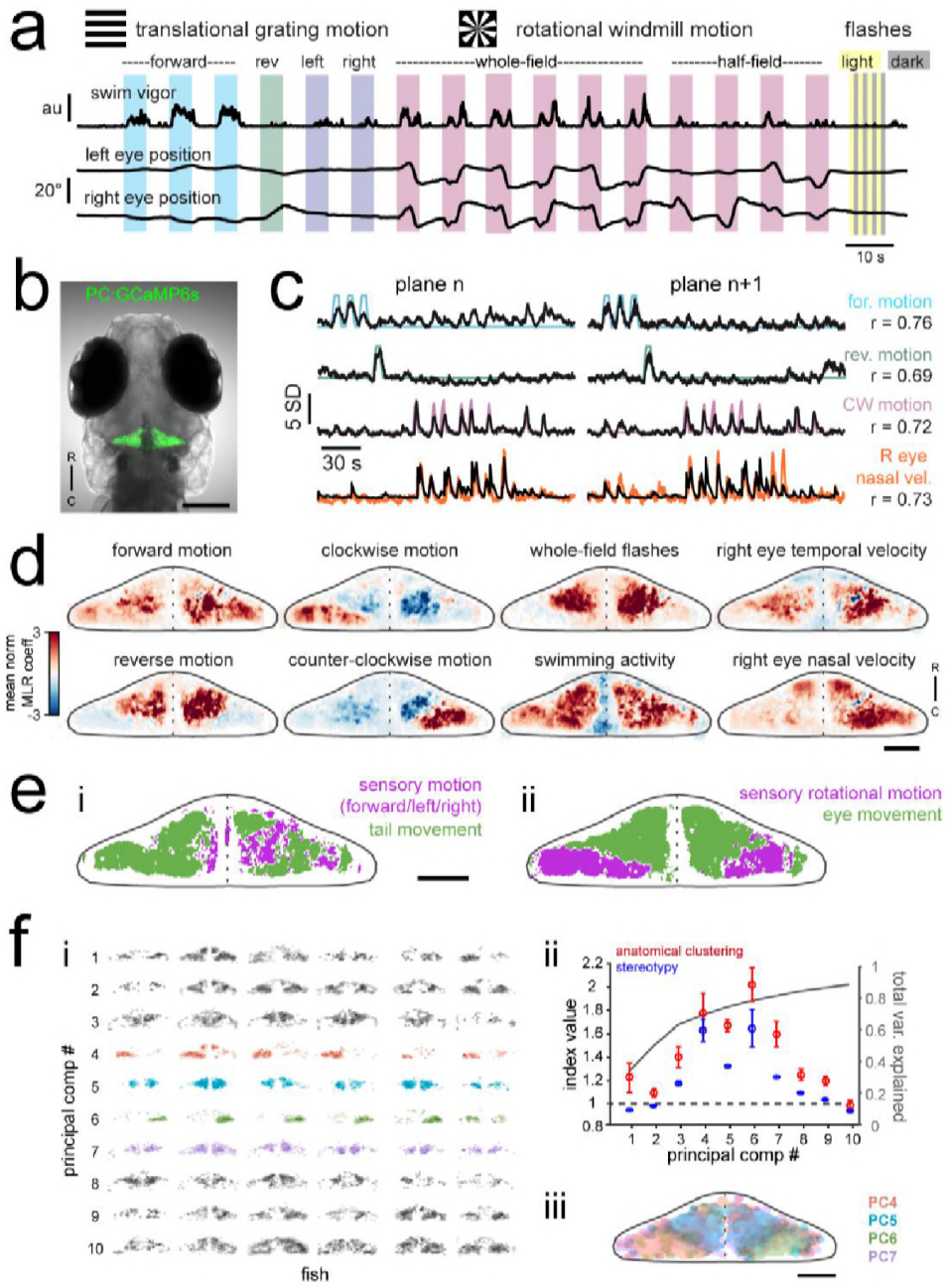

Figure 1. Purkinje cell activity is functionally clustered across the cerebellum.

a) Overview of the visual stimuli presented to the awake, behaving zebrafish during volumetric two-photon calcium imaging. See Methods for further details. The mean swimming activity and eye position for a representative fish across an entire experiment is shown (N=100 trials). b) Composite brightfield image of a 7 dpf zebrafish larvae from a dorsal view showing Purkinje cells expressing GCaMP6s driven by a ca8 enhancer element. Scale bar = 100 microns. c) Example z-scored fluorescent traces from Purkinje cells in this fish together with their best correlated sensory or motor regressors. Regressor and correlation coefficient is given at right for each cell. d) Heatmaps of the z-projected mean voxelwise correlation coefficients from multilinear regression (MLR) with example sensory and motor regressors for a representative fish (see Methods). Scale bar = 50 microns. e) Voxels from the example fish in d) are colored according to whether the best regressor for correlated sensory stimuli and motor events (including i) swimming and ii) eye

movement) are sensory (magenta), motor (green), or equal/uncorrelated (white). fi) Composite projections of the first ten principal components of Purkinje cell activity in response to experimental stimuli across all fish (N=6; see Methods), ordered in increasing variance explained. Colors are arbitrarily chosen. fii) Left axis, index values across the first ten principal components with respect to the anatomical clustering of principal components within a fish (red line) and the stereotypy of these clusters across fish (blue line). Dotted black line shows an index value of 1 or chance value: an index above this line denotes that the particular cluster is more anatomically clustered than expected by chance within fish (red) or more stereotypically anatomically located across fish than chance (blue). Right axis, total variance explained across principal components. fiii) Spatial map of the four principal components with the highest index values for both anatomical clustering within a fish as well as stereotypy across fish. See also Figures S1 and S6.

Individual fish showed segregated regions of Purkinje cell activity that correlated highly with different sensory and motor variables. Each different feature of the sensory stimulus or motor behavior, such as translational motion in a certain direction, or the duration of the swimming bouts across a trial, were used to build a vector of values for the trial duration. This vector was then convolved with a GCaMP kernel to produce a regressor for each feature (Figure 1c), and this set of regressors was evaluated against the calcium traces obtained from individual neurons to identify the feature(s) that each cell encoded (Figure 1d; Portugues et al., 2014).

Purkinje cell responses to reverse grating motion were concentrated rostromedially, while responses to luminance were located more centrally across both cerebellar hemispheres (Figure 1d). Both of these responses are predominantly sensory since these stimuli do not typically elicit behavioral responses in larval zebrafish (Figure 1a). The most caudolateral regions of the cerebellum were highly responsive to rotational motion, with Purkinje cells in the left hemisphere responding to clockwise motion and those in the right hemisphere responding to counter-clockwise motion (Figure 1d). In order to disambiguate the responses of Purkinje cells during visual stimuli that drive a specific behavior (translational motion and swimming, or rotational motion and left/right eye velocities), we performed voxelwise analysis to determine whether a sensory versus motor regressor was significantly better in explaining the activity in each voxel (Figure 1e; see Methods). The activity of Purkinje cells distributed across a broad region of the cerebellum correlated highly with tail movement during swimming whereas sensory grating motion was represented sparsely, in patches (Figure 1ei). In contrast, a large dense bilateral area of the caudolateral cerebellum correlated best with sensory rotational motion while the remaining area of the rostral and medial cerebellum was highly correlated with eye movements (Figure 1eii). These results indicate that locomotor activity of the tail and eyes is broadly encoded in Purkinje cell activity across the cerebellum whereas sensory responses are more clustered.

In order to understand Purkinje cell population activity beyond correlations with a particular stimulus or motor feature, we performed principal component analysis (see Methods). This approach allowed us to identify groups of Purkinje cells whose activity was modulated in a similar way during the experiment, regardless of what particular stimulus feature drove the response. This analysis revealed considerable spatial structure in Purkinje cell responses (Figure 1f). We used the first ten principal components (total fraction of variance explained = 0.9) to determine the anatomical clustering of functional responses within fish as well as the stereotypy of these clusters across fish (Figure 1f). These results reveal a clear spatial organization of Purkinje cells into functional regions across the zebrafish cerebellum.

Calcium signals in Purkinje cells report complex spikes with high fidelity with lesser contributions from simple spikes

Climbing fiber inputs driving complex spikes have been shown to reliably produce large dendritic calcium signals in mammalian Purkinje cells with little to no signal in the soma (Lev-Ram et al., 1992). In contrast, parallel fiber inputs may contribute to small, local calcium signals at dendritic spines or branchlets (see Kitamura & Kano, 2013 for review) while changes in sodium-dependent simple spike rates may be read out from somatic calcium signals (Ramirez & Stell, 2016). In order to understand how the signals obtained during calcium imaging relate to complex spike and simple spike output in larval zebrafish Purkinje cells, we obtained *in vivo* cell-attached electrophysiological recordings from single Purkinje cells expressing GCaMP6s (Figure S1).

As expected, we found that every complex spike elicited a peak in the calcium signal of a Purkinje cell's dendrites (Figure S1a,b). However, we also found that isolated bursts of simple spikes correlated with widespread increases in the dendritic calcium signal. Aligning the calcium signal to the onset of simple spike bursts and single complex spike events showed consistent simple spike-triggered calcium transients that were of smaller amplitude but a similar duration to complex spike-triggered transients (Figure S1b,d). These findings reveal that both complex spikes and simple spike bursts can contribute to the dendritic fluorescence signals obtained by calcium imaging in larval zebrafish Purkinje cells. We used regression methods to compare the contribution from complex and simple spikes to the fluorescence and saw that the majority of the contribution to these fluorescence signals comes from complex spikes, with the proportion from simple spikes varying across cells (mean contribution from complex spikes = 78.4 ± 6.8% , N=8 cells from 8 fish; Figure S1e,f). We furthermore observed that somatic signals and dendritic signals were highly correlated

(mean correlation = 0.87 ± 0.2, N=5 cells from 3 fish; Figure S1g,h), suggesting that the contribution from different inputs may not be as spatially segregated in these Purkinje cells as shown in other systems. Functional imaging data from Purkinje cell populations therefore reports both complex spikes and high frequency simple spiking.

Electrophysiological recordings from Purkinje cells reveal distinct complex spike responses that can be grouped into four primary response types corresponding to sensory or motor responses

In order to overcome the ambiguous contribution of complex spikes versus simple spike bursts to calcium signals, we performed cell-attached Purkinje cell electrophysiological recordings at different locations across the cerebellum in the awake, paralyzed larval zebrafish while presenting visual stimuli as for the functional imaging experiments described above (N = 61 cells from 61 fish). Complex spikes and simple spikes can be clearly distinguished in these recordings with automated thresholding by amplitude (Figure 2a) and converted to a spike rate (Figure 2b; see Methods). Simultaneous fictive recordings of locomotor activity were obtained from a ventral root extracellular electrode (Figure 2a) as previously described (Masino & Fetcho, 2005) and used to extract information about fictive swim bouts (see Methods). It should be noted that visually-driven motor behaviors are robust on average but episodic and variable across trials, allowing us to clearly disambiguate sensory and motor contributions to neuronal activity. Fish swim in episodic bursts of swimming that last just hundreds of milliseconds, separated by rest periods lasting seconds, whereas the visual stimuli driving these swim bouts were presented for many seconds. As a result, the motor regressors for swimming activity look very different from visual (sensory) regressors (Figure S2) and are only moderately correlated with these stimuli on a trial by trial basis (mean correlation = 0.31 ± 0.2, Figure 2c).

In an approach similar to that used to analyze our functional imaging results, we built regressors to capture the most salient features of the visual and motor stimuli (Figure 2d and Figure S2). Evidence suggests that zebrafish Purkinje cells receive only one climbing fiber input from the inferior olive by 7 days post fertilization (dpf) (Hsieh et al., 2014, 2018), however mixed complex spike responses to multiple stimuli are possible due to mixed selectivity (multiplexing) in neurons of the inferior olive (Ohmae & Medina, 2015) or residual multiple climbing fiber input. Least-squares multilinear regression was used to calculate coefficient weights for the complex spike activity of all cells with these regressors (Figure 2e and Figure S2; see Methods).

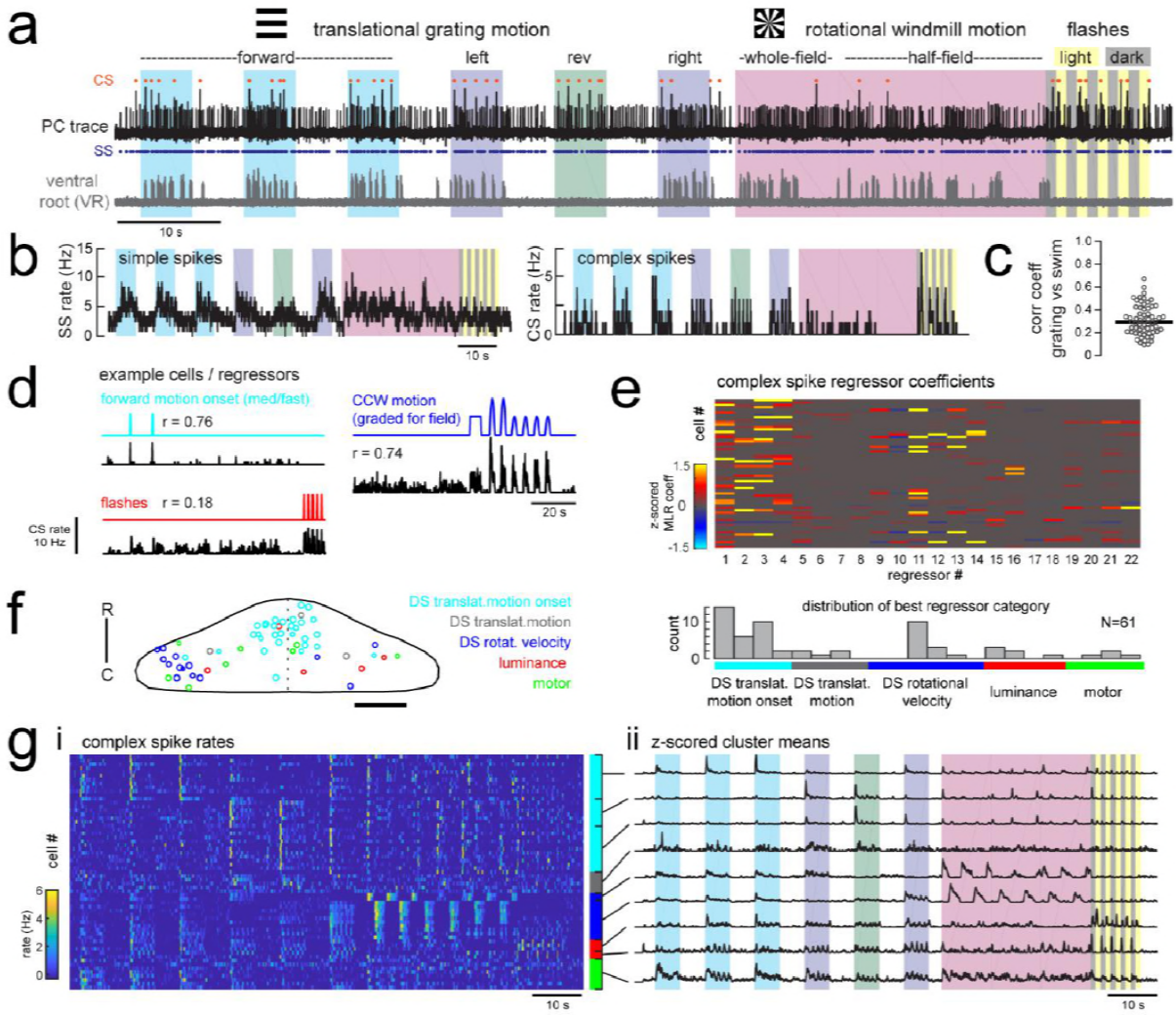

Figure 2. Electrophysiological recordings from Purkinje cells reveal distinct complex spike responses that can be grouped into four primary response types corresponding to sensory or motor features.

a) Example single trial from a cell-attached Purkinje cell (PC) recording (upper trace, black) with simultaneous ventral root recording (lower trace, gray, shown as a moving standard deviation). Complex spikes in the PC are indicated by orange dots above the trace and simple spikes are indicated by blue dots below the trace. Stimuli are color-coded as before (see Figure 1 and methods for more details). b) Left, the mean simple spike (SS) and complex spike (CS) rate for the cell shown in (a) across five trials. Right, the correlation coefficients of forward, left and rightward grating motion with the trialwise and average fictive swim activity for all fish. c) Plot of the correlation coefficient for each fish between the regressor for concatenated swimming activity during moving forward, left, and right gratings across all trials and the summed sensory regressor for forward, left, and right grating motion. The mean is indicated by the black bar. d) Example mean complex spike rates and example regressors e) Above, heatmap of coefficient weights for the complex spike firing rates of 61 cells from z-scored least-squares multilinear regression (MLR) with a full set of 24 stimulus- and motor-related variables (see Methods). Below, histogram showing the distribution of cells' highest regressor weight. f) Location of these cells across all fish mapped onto a reference cerebellum (bird's eye view). The color indicates the highest MLR coefficient weight for that cell while the size indicates the degree to which that coefficient contributes to the overall firing rate respective to the others, where the biggest circles = 100%. Scale bar = 50 microns. g) Left, heatmap of complex spike rates for all 61 cells clustered according to their highest MLR coefficient weight. To reduce extraneous clusters, all motor-related responses are grouped in

one cluster and some luminance-related regressors were combined. Colored bars at right indicate complex spike phenotype as indicated in previous panels. Right, the mean z-scored complex spike rate from each cluster. See also Figure S2.

We observed that complex spikes generally responded to a narrow subset of stimuli, as shown by the sparse matrix of regressor weights (Figure 2e). Only a few sensory or motor features provided a significant contribution to each cell's complex spike rate (mean number of nonzero coefficients = 6.0 ± 0.4 / 22, N=61). A survey of the best regressor category for each cell from this dataset revealed that Purkinje cell complex spike responses were most strongly enriched for visual information, specifically the onset of direction-specific translational motion (N=31/61) and the direction-specific rotational velocity (N=14/61). The remaining Purkinje cells were categorized as having complex spikes that best responded to changes in whole-field luminance, to fictive motor activity, or to the duration of translational motion (Figure 2e). Notably, sensory responses are far better represented than motor responses in the complex spike responses of Purkinje cells, despite the fact that many of the visual stimuli we used elicited robust swimming behavior. Only 8/61 cells had the biggest contribution to complex spike rates from motor activity, and across the remaining cells the average contribution from motor regressors was less than 5% (3.7 ± 1%, N=53). Of the eight cells whose best regressor was motor-related, there were nonetheless significant responses to visual features present as determined by non-zero sensory coefficient weights accounting for 10-40% of the complex spike activity (mean contribution = 20 ± 5%).

We hypothesized that the specificity of complex spike sensory responses across Purkinje cells could underlie the spatial clustering we observed with functional imaging. Mapping the coordinates of all Purkinje cells onto a reference cerebellum revealed a spatial organization of complex spike sensory response phenotypes similar to our functional imaging data (Figure 2f and Figure 1d). In particular, we observed a rostromedial cluster of cells responsive to the onset of directional motion in the visual stimulus and a caudolateral cluster of cells responsive to rotational stimulus velocity. Luminance responses were more scattered but generally occupied the central zone between these regions. Closer inspection of the complex spike firing rates across cells reveals that these responses can be further subdivided based on the specific type of response to the stimulus. For example, direction-selective motion onset-responsive Purkinje cells differ in their directional tuning, and luminance-responsive cells can prefer either increases or decreases in luminance, or bidirectional changes (Figure 2g).

Together with our functional imaging data, these results suggest that nearly all zebrafish Purkinje cells contribute to the formation of three distinct spatial regions across the cerebellum through sensory complex spike profiles encoding either directional translational motion onset, rotational motion, or luminance of the visual world. We performed further detailed electrophysiological and anatomical analyses of the Purkinje cells from each of the three sensory response types in order to examine what aspects of the sensory stimuli were encoded by their complex spikes and in turn where they send their outputs.

Purkinje cells in different regions receive climbing fiber input related to different, specific visual features and send outputs to different downstream regions

The largest group of Purkinje cells showed strong, direction-selective responses to the onset of translational motion, as revealed by significant correlation weights for these regressors (see Methods; N=33/61 cells). These responses typically spanned two of the four cardinal directions tested, producing on average just one complex spike at the onset of motion in the preferred directions (1.2 ± 0.6 spikes/stimulus; Figure 3a). The direction selectivity index (DSI) of these cells ranged from 0.2-0.9 and no cells were found that responded significantly to motion onset in opposing directions (Figure 3a and Figure S3a). Although these Purkinje cell somata are closely clustered in the most rostromedial part of the cerebellum (Figure 1d), the lateralization of Purkinje cells was biased such that cells in the left cerebellar hemisphere preferred either forward motion to the right (0 to 90°, N=7) or reverse motion to the left (-90 to -180°, N=5; Figure S3a). Conversely, Purkinje cells in the right cerebellar hemisphere preferred either forward motion to the left (0 to -90°, N=5) or reverse motion to the right (90 to 180°, N=5; Figure S3a).

The second group of Purkinje cells, located in the caudolateral cerebellum, showed a large increase in complex spikes during either clockwise or counter-clockwise rotational motion that persisted throughout the duration of movement (Figure 3b; N=12/61 cells). As seen in our functional imaging data (Figure 1c), responses to rotational motion were highly lateralized such that all Purkinje cells (10/10) that preferred clockwise rotational motion were located in the caudolateral region of the left cerebellar hemisphere while the only two Purkinje cells that preferred counter-clockwise motion were located in the mirror symmetric region of the right cerebellar hemisphere (Figure S3b). Clockwise motion-preferring cells also show an increase in complex spiking for the duration of rightwards translational motion whereas counter-clockwise motion-preferring cells respond to leftwards translation motion (Figure S3b), suggesting that these cells integrate motion over a large

area situated in the front half of the visual field. During rotational motion in the preferred direction, complex spike firing rates in these cells were two to five times higher than baseline (mean rate increase = 340 ± 40%, N=12). In contrast, complex spike rates during motion in the non-preferred direction fell to nearly zero, well below the baseline rate (mean rate non-preferred direction = 0.32 ± 0.1 Hz versus 0.87 ± 0.1 Hz at baseline; Figure S3b). Complex spike rates for translational motion in the preferred direction followed a similar pattern (mean rate increase above baseline = 280 ± 20%). We also observed an apparent homeostatic regulation of complex spikes in these cells where spontaneous firing rates were strongly depressed for several seconds following the robust complex spike responses during this stimulus period (Figure 2d,g).

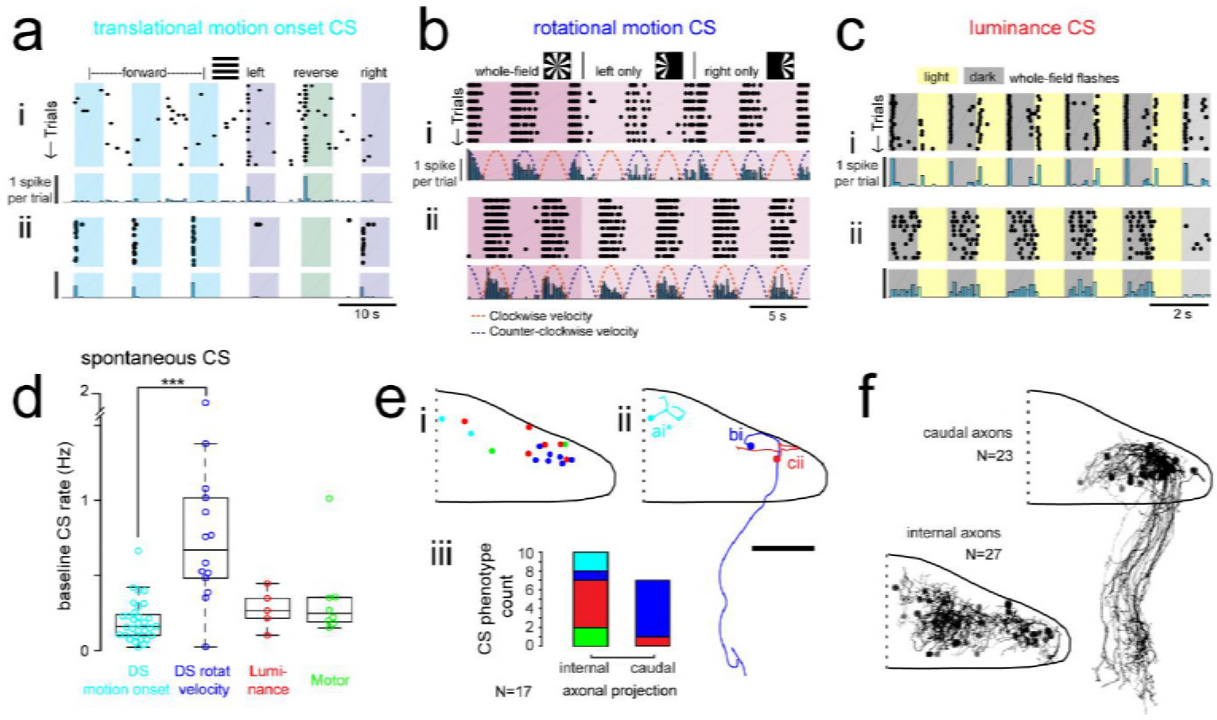

Figure 3. Purkinje cells in different regions show complex spike responses that encode different visual features and send outputs to different downstream regions

a) Raster plot (upper left panels) and histogram (lower left panels, 500 ms bins) of complex spikes occurring across trials during translational whole-field motion of black and white bars in all four cardinal directions for two example cells. See also Figure S3. b) Raster plot (upper left panels) and histogram (lower left panels, 100 ms bins) of complex spikes occurring across trials during whole- and half-field bidirectional rotational motion of a black and white windmill for an example cell. The dashed lines over the histogram show the velocity of the stimulus in each direction across the trial. See also Figure S3. c) Raster plot (upper left panels) and histogram (lower left panels, 100 ms bins) of complex spikes occurring across trials during whole-field light/dark flashes for two example cells, i) and ii). See also Figure S3. d) A box plot of complex spike firing rates during blank trials (no visual stimuli) for cells grouped by their sensory or motor complex spike category

(see Fig 2). N = 31, 14, 5, 8. Asterisks indicate significance (one-way ANOVA with Bonferroni post hoc correction, p<0.001). j i) The location of cells colored by complex spike phenotype are plotted onto a flattened bird's eye view of the cerebellum with all coordinates flipped to the right half of the cerebellum. e ii) Three example maximum projection images of traced axonal morphology from stochastically-labelled, Fyn-mClover3-expressing Purkinje cells for which electrophysiological recordings were also obtained. Labels for each cell refer to the electrophysiological traces in previous panels. The asterisk for cell a) indicates that these coordinates were flipped to the right half of the cerebellum. Scale bar = 50 microns. e iii) Categorical grouping of complex spike phenotypes for internal versus caudal axonal projections. N = 17 cells from 17 fish. f) Morphed Purkinje cell axonal morphologies from single-cell labelling across fish (N=50 cells) can be grouped into two populations based on axonal projection (as for e iii). N=27 cells with internal axons, N=23 cells with caudal axons.

The third prominent group of Purkinje cells had complex spike responses correlated with changes in whole-field luminance. These were identified using autocorrelation analyses to periodic whole-field flashes (Figure S3c; see Methods) and included some Purkinje cells belonging to the previous sensory groups responsive to visual motion (N=25/61 cells with significant autocorrelation to flashes; Figure 3c and Figure S3c-e). Purkinje cells within this group had complex spike responses that encoded either luminance increases (9/25) or decreases (11/25) or both (5/25; Figure 3c and Figure S3d). The latency from the onset of the preferred luminance transition to the first complex spike occurred for each cell with very little jitter but the latency itself varied across cells (Figure S3d). This group of Purkinje cells showed a wide distribution in their localization across the central region of the cerebellum (Figure S3e). Luminance-responsive Purkinje cells in many but not all cases also showed significant complex spike responsive to local luminance changes during the translational motion of gratings (Figure S3f), suggesting that some cells may have smaller receptive field sizes over which they integrate luminance. Most responses were transient such that cells fired just one complex spike for the preferred luminance change (mean = 0.80 ± 0.02 spikes). We did however observe sustained changes in complex firing rates in two cells that persisted as long as the duration of the preferred luminance and therefore appear to encode ambient luminance through their complex spike rate (Figure 3cii, one-way ANOVA with Bonferroni post hoc correction, p<0.01; Figure S3g,h) .

Notably, the spontaneous complex spike rates were quite different between these groups. Purkinje cells responding to rotational motion velocity had a significantly higher baseline firing rate than those with directionally selective motion onset responses (0.77 ± 0.1 Hz and 0.20 ± 0.02 Hz, respectively, p<0.001, Bonferroni post hoc correction; Figure 3d). Purkinje cells responding most strongly to luminance or motor activity had intermediate baseline complex spike rates (0.28 ± 0.1 Hz and 0.34 ± 0.1 Hz, respectively; Figure 3d).

Mapping the coordinates of Purkinje cell somata belonging to these three complex spike sensory subtypes supports a regional division of the cerebellum along the rostrocaudal axis where each of the three regions within the cerebellar hemisphere receives inputs from the same or similar inferior olive neurons carrying visual information (Figure 3ei). To examine the outputs of Purkinje cells, we performed cell-attached electrophysiological recordings with morphological analyses via stochastic single-cell labelling of Purkinje cells to visualize the axonal projections (N=17 cells from 17 fish; Figure 3eii). Unlike the mammalian cerebellum, where all Purkinje cell axons project outside of the cerebellar cortex, zebrafish Purkinje cells can be divided into two anatomical populations - one with internally-projecting axons that contact eurydendroid cells (the equivalent of mammalian cerebellar nuclei neurons) and the other whose somata are more lateral and who have externally-projecting caudal axons that contact neurons in the vestibular nuclei (Bae et al., 2009; Matsui et al., 2014). Strikingly, 6/7 Purkinje cells with caudally projecting axons exhibited a clear complex spike phenotype for directional rotational motion, whereas only 1/10 cells with an internal axon had this same phenotype (Figure 3eiii). We further reconstructed and aligned 50 singly-labelled Purkinje cell morphologies across fish. Although the somata of Purkinje cells with caudal (N=23/50) and internal (N=27/50) axons partially overlap, the segregation of rotational motion responses with caudal axon anatomies in this dataset further support our definition of this Purkinje cells functional region (Figure 3e). We also found that Purkinje cell dendrites generally had a classic albeit simplified morphology with mostly planar dendrites (Figure S4) oriented orthogonally to the axis of parallel fiber extension across the cerebellum (Knogler et al., 2017), as seen in mammalian cerebellum (Eccles et al., 1967).

Together, these results define three functional regions of Purkinje cells across the cerebellum operating with different complex spike frequencies and encoding distinct sensory features related to visuomotor behaviors, of which one region also send the majority of its projections to a different downstream area than the others.

Motor-related complex spikes are rare

As discussed above, motor regressors did not significantly contribute to complex spike activity in the majority of Purkinje cells (N=47/61), despite an abundance of visually-evoked fictive behavior. Eight cells had the largest regressor weight for their complex spike activity from a motor regressor while four additional Purkinje cells had small but nonzero regressor coefficient weights, therefore a total of twelve cells were included for further motor analysis. We analyzed motor-related complex

spike responses from these cells during spontaneously-evoked swimming in blank trials as well as trials where visual stimuli elicited swimming in order to confirm that responses were indeed driven by motor activity and not sensory stimuli (Figure S5a). Motor-related complex spikes had considerable jitter from bout onset in blank trials in contrast to the fixed latencies for most sensory-driven complex spikes (Figure S5b, compare with Figure 3). This is consistent with observations that complex spikes show no phase-locking with stereotyped locomotor movements (Apps, 1999). Some Purkinje cells also showed an increase in complex spikes following bout offset (Figure S5c). Notably, the mean swim bout-related complex spike rate was higher for spontaneous bouts in blank trials that for visually-driven bouts (Figure S5a,c; $p<0.05$, Wilcoxon signed rank test, N=12 cells). This finding aligns with several studies showing that sensory and motor signals can interact to alter climbing fiber input to the cerebellum via the inhibition of inferior olive activity from cerebellar nuclei, the red nucleus, and other indirect pathways (see Apps, 1999, and Gibson et al., 2002 for reviews).

Of the cells that showed a motor-related change in complex spike activity, the majority had an increase in complex spikes during a fictive bout (N = 9/12; Figure S5d). These responses were however unreliable and a complex spike occurred on less than half of bouts on average (mean probability = 0.38 ± 0.07 for stimuli trials, N=9 cells; mean probability for blank trials = 0.42 ± 0.07, N=5 cells). The remaining three cells showed a decrease in complex spikes during fictive bouts (mean probability of a complex spike during bout < 0.02, N=3; Figure S5d). Unlike the spatial mapping seen for Purkinje cells sensory response types, Purkinje cells with motor-related complex signals were distributed across the cerebellum with no apparent clustering (Figure S5e).

We observed that both translational and rotational motion induced frequent bouts of fictive swimming in fish (Figure 2a), however the complex spike responses during these stimuli in most Purkinje cells did not correlate well on a trial-by-trial basis with fictive swimming bouts and were thus classified as sensory, as described above. Rotational windmill stimuli are however known to evoke stereotyped eye movements known as the optokinetic reflex (Easter & Nicola, 1996), therefore complex spike responses to rotational visual motion could relate to eye movement. Studies of the cerebellar control of eye movements have shown evidence that climbing fibers provide eye motor error signals, which could account for the prominent complex spike signals observed in Purkinje cells in the caudolateral cerebellum during rotational windmill motion. In order to examine the potential contribution of eye movement to driving complex spikes in this group of Purkinje cells, we performed cell-attached recordings from Purkinje cells in the caudolateral cerebellum in the semi-paralyzed zebrafish, where the eyes were free to move and were tracked

with a high-speed camera (see Methods). The independent movement of each eye was then used to build a set of twelve regressors corresponding to eye position and velocity in different directions (Figure S5f).

Least-squares multilinear regression was used to calculate coefficient weights for the complex spike activity of all cells with the previously described eighteen sensory regressors and these twelve new eye motor regressors. We found that simple spike phenotypes across cells were strongly motor whereas we once again observed a clear bias for a sensory complex spike phenotype across Purkinje cells (N=11/13), with only two cells whose best regressor related to eye movement (Figure S5g,h). A further analysis of the complex spike phenotypes of these latter two cells showed that in one case, the eye movement was so well-correlated with the sensory stimulus that it was hard to disambiguate the true sensory vs motor nature of the complex spike response (Figure S5i, cell 2). For the other cell (Figure S5i, cell 3), a strong luminance (sensory) complex spike phenotype was identified through additional autocorrelation analyses ($p<0.001$ from Ljung-Box Q-test; $r=0.67$ for correlation with the luminance regressor) in addition to the moderate correlation with eye movement ($r=0.32$ for correlation with eye motor regressor). Nonetheless, the majority of Purkinje cells in this region could be clearly assigned to a sensory complex spike phenotype since these cells showed very stereotyped complex spike responses to directional rotational stimuli that did not correlate well with the variable eye movements observed across trials (Figure S5j,k). We conclude from these data that the complex spike responses during rotational visual motion are predominantly sensory rather than motor. Furthermore these responses are likely not error signals due to lack of eye movement because these signals are equally prominent in the paralyzed fish as in the electrophysiological and functional imaging experiments where the eyes are free and track the stimulus (Figure 1d,e).

Simple spike responses across the Purkinje cell population are highly modulated by motor efference copies during fictive swimming

Having observed that Purkinje cells can be clustered into functional regions defined by their sensory complex spike responses and anatomical features, we next wanted to understand how simple spike responses were organized across the cerebellum. Sensory and motor contributions to simple spike responses in individual Purkinje cells were much more broadly distributed than those observed for complex spike activity (Figure 4a and Figure 2d), as expected in a circuit where many parallel fibers converge on a single Purkinje cell (De Zeeuw et al., 2011). The regression analyses revealed that

translational and rotational motion of visual stimuli, regardless of direction, was the most prominent sensory feature encoded by simple spike activity as evidenced by the broad distribution of moderate coefficient weights for individual cells across motion regressors in most or all directions (Figure 4a). These findings suggest that Purkinje cells are integrating inputs from motion responsive granule cells with different directional tuning (Knogler et al., 2017).

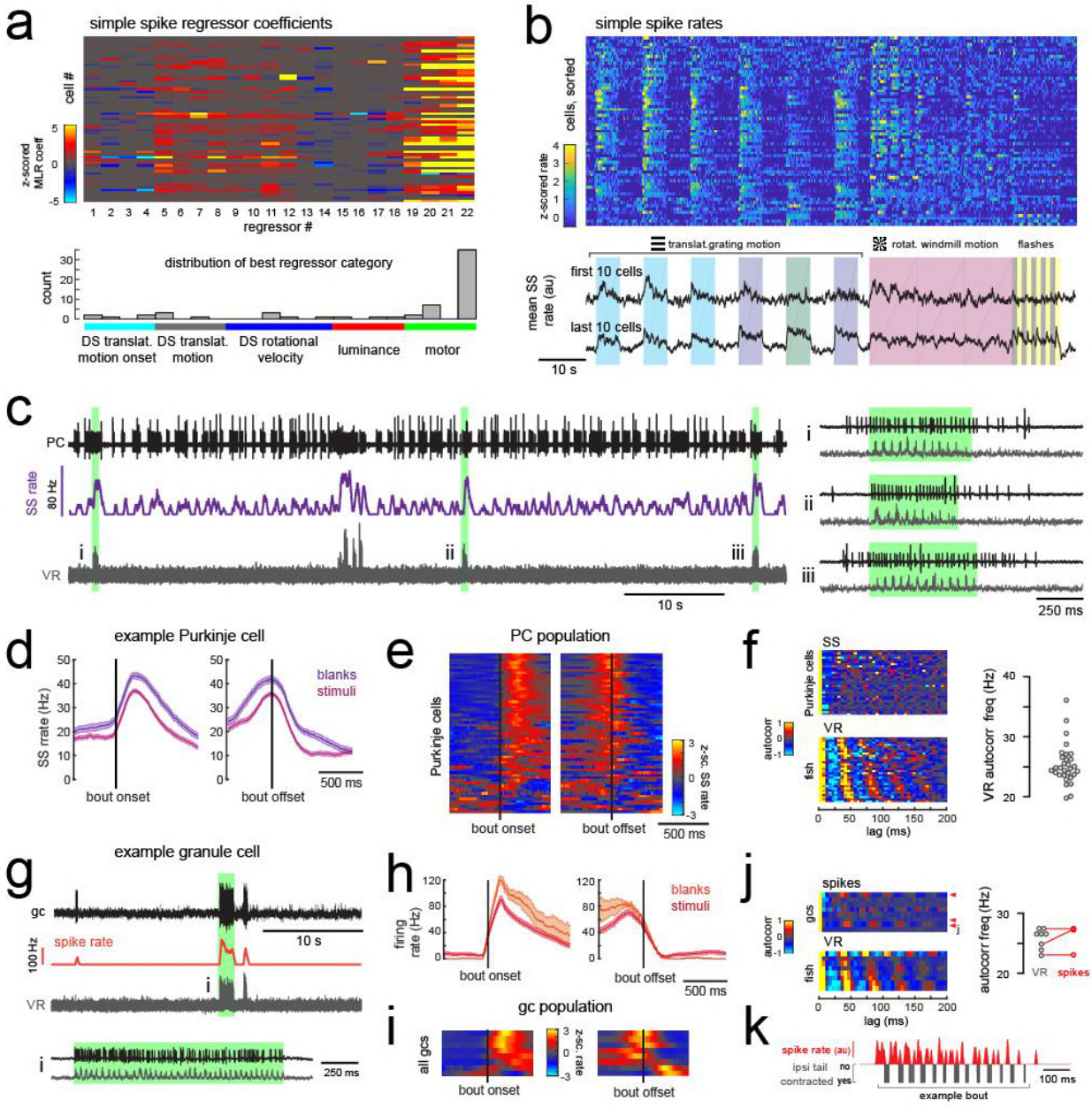

Figure 4. Simple spike rates in Purkinje cells and in granule cells are increased during fictive swimming

(legend continued on next page)

a) Above, heatmap of coefficient weights for the simple spike firing rates of 61 cells from least-squares regression with a full set of 24 stimulus- and motor-related variables (see methods for more details). Below, histogram showing the distribution of cells' highest regressor weight and the associated sensory/motor categories. b) Upper panel, heatmap of z-scored simple spike rates for all 61 cells sorted by decreasing motor coefficient weight. Lower panel, the mean simple spike rate for the ten cells with the highest (upper trace) and lowest (lower trace) motor coefficient weights. c) Left panel, example cell-attached Purkinje cell recording (PC, upper trace, black) from a blank trial (no stimuli) with simultaneous ventral root recording (VR, lower trace, gray, shown as a moving standard deviation). The simple spike rate is also shown (SSrate, middle trace, purple). Right, the bouts highlighted in green on an expanded timescale show the close timing of fictive bout onset and simple spike activity. d) The bout on- and off-triggered mean simple spike firing rates for the cell in c) during blank recordings (purple) and stimulus trials (pink). e) Z-scored heatmap of bout on- and off-triggered mean simple spike firing rates across all Purkinje cells sorted by mean firing rate in the 300 ms following bout onset. f) Mean autocorrelation heatmap for simple spikes (SS, upper panel) and for ventral root recordings (VR, lower panel) for all Purkinje cells that showed spontaneous swimming bouts during blank trials (N=30 cells from 30 fish), sorted by time to first peak in the VR autocorrelation. Right, the first significant peak in the VR autocorrelation for each recording is plotted to give the mean fictive swim frequency for each fish. g) Upper panel, example cell-attached recording from a granule cell (gc, upper trace, black) from a blank trial with simultaneous ventral root recording (VR, lower trace, gray). The granule cell firing rate is also shown (spike rate, middle trace, orange). The bout highlighted in green (i) is shown below on an expanded timescale. h) The bout on- (left) and off- (right) triggered mean firing rates for this granule cell during blank recordings (orange) and stimulus trials (red). i) Z-scored heatmaps of bout on- (left) and off- (right) triggered mean firing rates in all granule cells sorted by mean firing rate in the 300 ms following bout onset (N=8 cell from 8 fish). Timescale same as for upper panels. See also Figure S7. j) Mean autocorrelation heatmap for spikes (upper panel) and ventral root recordings (VR, lower panel) for all granule cells from i), sorted by time to first peak in the VR autocorrelation. The red arrowheads signify granule cells with significant spike autocorrelations during fictive swim bouts (N=3; $p<0.001$, Ljung-Box Q-test; see Methods). Right, the first significant peak in the VR autocorrelation for each recording is plotted to give the mean fictive swim frequency for each fish. The red circles are the mean spike autocorrelation frequency obtained from the three significantly autocorrelated granule cells. k) An example bout from the cell indicated in j), which was located ipsilateral to the ventral root recording. The smoothed spike rate (red) is in antiphase with the ipsilateral fictive tail contractions (grey).

Although simple spike rates were modulated to some extent by many of the visual stimuli presented, motor activity significantly modulated simple spike activity in nearly all Purkinje cells across the cerebellum (N=60/61) and was in fact the main contributor to modulating simple spike activity in the majority of cells (N=44/61; Figure 4a). Simple spike firing rates for these cells were consistently better correlated with bout vigor (equivalent to swim "strength", calculated from the standard deviation of the tail amplitude) than bout duration, suggesting that fictive swimming activity is encoded in a graded manner by simple spike output. Mean simple spike firing rates across the population were on average twice as high during a bout as during the rest of the trial (mean rate during a bout = 14.5 ± 1.5 Hz vs 7.6 ± 0.8 Hz at rest; $p<0.001$, Wilcoxon signed rank test). Trial-averaged simple spike responses across the population appeared as a continuum rather than as clusters (Figure 4b), suggesting that the organization of parallel fiber inputs does not follow the regional specificity of climbing fiber inputs and send similar information across the entire Purkinje cell layer.

In order to rule out potential sensory contributions to simple spike rates during visually-evoked behaviors, we analyzed simple spike activity during additional blank trials without visual stimuli (Figure 4c). Purkinje cells exhibit considerable spontaneous simple spike firing in the absence of any sensory stimuli or motor activity due to intrinsic bistability (Sengupta & Thirumalai, 2015), however fictive swim bouts consistently increased simple spike firing well above baseline levels (Figure 4c-e) and to an ever greater extent for spontaneous bouts in the absence of visual stimuli ($p<0.01$, Wilcoxon signed rank test). Aligning the mean bout-triggered simple spike rates for all Purkinje cells at bout onset and offset confirmed that the majority of cells have consistent motor-related increases in simple spike activity that begin at bout onset and return to baseline following bout offset (Figure 4e) although a small number of Purkinje cells instead show bout-triggered decreases in simple spike firing rates (Figure 4e), as observed elsewhere (Scalise et al., 2016). As expected for rhythmic locomotor output, the ventral root signal was highly autocorrelated for all fish with a mean autocorrelation frequency across fish of 26.7 ± 0.7 Hz (N=30 fish; Figure 4f), consistent with the slow swim bout frequency reported for restrained zebrafish larvae (Severi et al., 2014). The autocorrelation analyses of simple spike firing for each Purkinje cell during a spontaneous fictive bout revealed however no significant autocorrelations for simple spikes at any frequency. Unlike the modulation of simple spike firing rate seen during step phase in locomoting rats (Sauerbrei et al., 2015), simple spikes in zebrafish Purkinje cells do not appear to be modulated in phase with rhythmic swimming activity but are nonetheless graded by swim strength. This suggests that individual Purkinje cell firing does not encode the activation of individual muscles involved in rhythmic swimming.

Motor activity is broadly represented in granule cell signals

The timing and reliability of swim-related simple spike activity is consistent with motor efference signals from spinal locomotor circuits arriving along mossy fibers to the granule cell layer, and subsequently to Purkinje cells, during fictive swimming. A disynaptic pathway from spinal premotor interneurons to the granule cells via the lateral reticular nucleus was recently found that would convey information about ongoing network activity in the spinal cord (Pivetta et al., 2014). Furthermore, extensive electrophysiological recordings from the granule cells of the cerebellum-like circuit of the electric organ in the electric fish revealed that an overwhelming majority (>90%) of granule cells receive depolarizing motor efference signals during electric organ discharge, although this translated into spiking in only ~20% of granule cells (Kennedy et al., 2014).

In order to characterize motor-related granule cell activity and its potential contribution to motor-related excitation in Purkinje cells, we imaged responses in the granule cell population to the same set of visual stimuli while tracking tail and eye movement (Figure S6). Multilinear regression was once again used to disambiguate responses to sensory stimuli and motor activity. Across fish (N=7), we observed that granule cell activity was strong and widespread during swimming activity, both in the somatic layer and across the parallel fiber layer (Figure S6). Granule cell activity relating to eye movements was weaker but also widespread (Figure S6). These findings suggest that a large number of granule cells receive mossy fiber inputs relaying motor efference copies that drive them to fire, and they in turn drive broad motor-related activation of simple spikes in Purkinje cells (Figure 1). These findings show more widespread motor-related representations in comparison to previous population-wide analyses of granule cell activity (Knogler et al., 2017) due to the abundance of behavior elicited by the current set of visual stimuli.

In order to better understand the temporal patterning of swim-related motor signals in the granule cells layer, we performed additional electrophysiological recordings from randomly targeted granule cells across the cerebellum while simultaneously recording ventral root activity to identify fictive swim episodes. These recordings revealed several granule cells with negligible firing rates in the absence of motor activity but that showed large, significant increases in their spike rates during fictive bouts (N=6/8 cells; mean firing rate at rest = 1.3 ± 0.3 Hz vs 25.7 ± 7.6 Hz during a bout; $p<0.005$, Wilcoxon signed rank test; Figure 4-i and Figure S7). These granule cells could reach high instantaneous firing frequencies of up to 150 Hz during a fictive bout, similar to the burst firing seen in mammalian granule cells during locomotion (Powell et al., 2015) or whisker stimulation (van Beugen et al., 2013). Half of these motor-excited granule cells (N=3/6) also showed significant autocorrelations in their spiking activity during fictive swimming ($p<0.001$, Ljung-Box Q-test; Figure 4j). The frequency of the spike autocorrelations for these cells was comparable to the fictive swim frequency obtained from the ventral root (mean difference in frequency = 1.3 ± 0.6 Hz, N=3), suggesting that the periodicity of granule cell spiking is related to the swimming activity (Figure 4i). The phase of the granule cell spiking with respect to the ipsilateral ventral root activity varied however across cells, arriving either in phase, with a lag, or in antiphase (Figure 4k).

Together, these results suggest that motor efference copies are relayed along mossy fibers to many granule cells to drive burst firing during swimming bouts, whether fictive or real. In turn, parallel fibers deliver swim-related excitation to nearly all cerebellar Purkinje cells. The widespread increases in Purkinje cell calcium signals observed in the behaving animal during swimming (Figure

1d) therefore are likely to reflect simple spike bursts in Purkinje cells (Figure S1) driven by the high frequency firing of one or more presynaptic granule cells.

Purkinje cells combine sensory and motor information from distinct inputs

Our data suggests that as a population, Purkinje cells preferentially encode visual features in their complex spike activity whereas swimming activity, arriving in the form of motor efference copies, is predominantly encoded by simple spikes. Breaking this down by group, we find that Purkinje cells belonging to the three sensory complex spike groups described above have simple spike activity that is correlated most strongly with motor activity (fraction of total signal from motor regressors = 0.65 ± 0.05, 0.54 ± 0.07, 0.76 ± 0.02 for the three CS sensory phenotypes; Figure 5a). In contrast, for the small group of Purkinje cells with dominant motor-related complex spike phenotypes, the contribution from motor activity to simple spike responses is relatively low (0.35 ± 0.12) and simple spikes are instead broadly influenced by a combination of sensory and motor features (Figure 5a). This relationship holds true for individual Purkinje cells as well (Figure 5b). Together, these data suggest that sensory and motor information is combined in Purkinje cells from distinct sources.

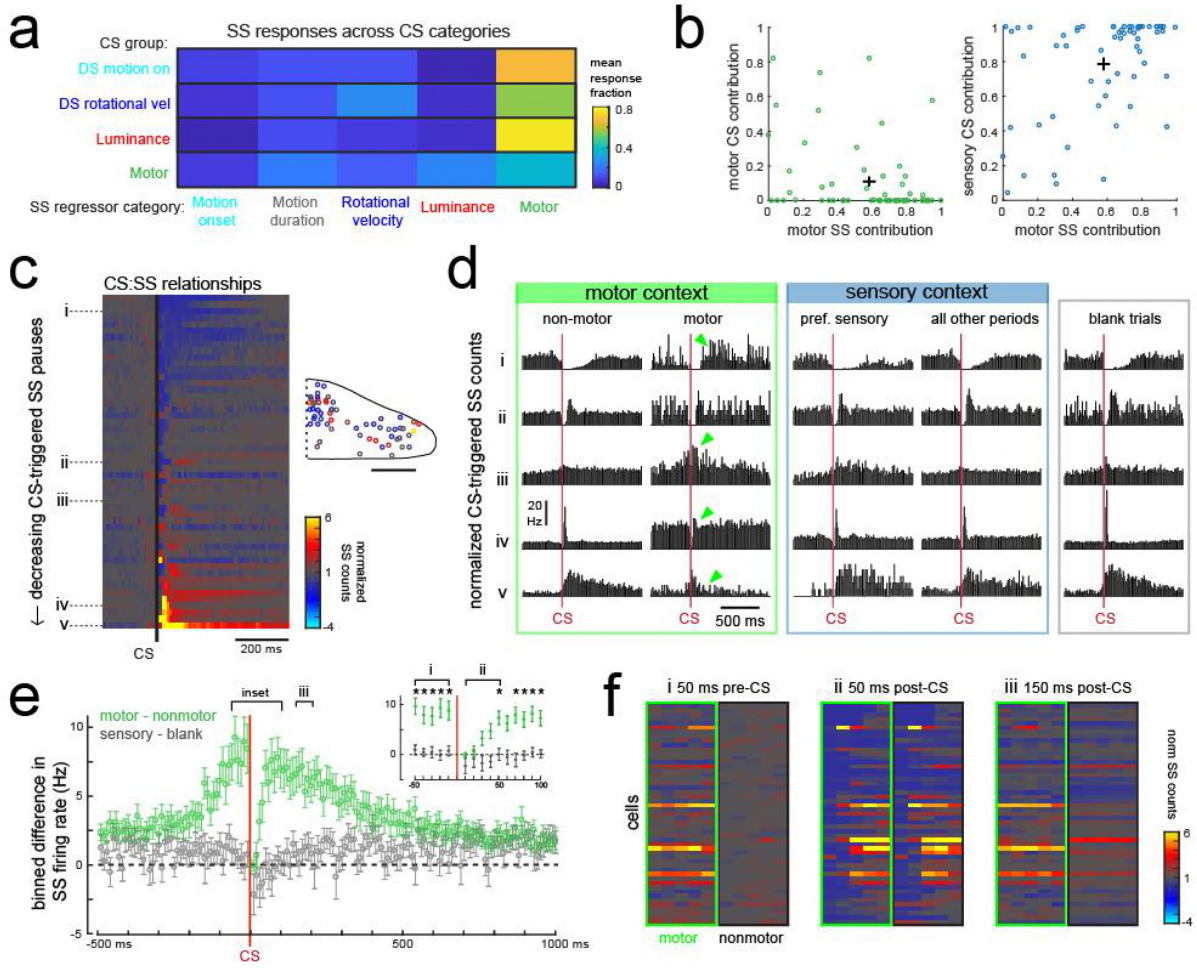

Figure 5. Individual Purkinje cells combine sensory and motor information and modify their simple spike output in a complex spike- and motor context-dependent way

a) The mean fraction of the simple spike (SS) response contributed by each regressor computed for each of the four Purkinje cell complex spike (CS) groups. b) Left, scatterplot of the fraction of complex spike versus simple spike activity accounted for by motor regressors. Right, the fraction of simple spike activity accounted for by motor regressors versus the fraction of complex spike activity accounted for by all sensory regressors. c) Heatmap of simple spike counts for each cell normalized to the 100 ms preceding a complex spike for all cells sorted by decreasing simple spike pause and increasing excitation. Simple spike counts for each cell (row) are normalized to the mean simple spike count in the 100 ms preceding a complex spike. The inset shows the location of these cells colored by the normalized difference in simple spiking in the 50 ms following the CS. d) The mean CS-triggered SS count (10 ms bins) is shown for five example cells (as indicated in c) for five different contexts. Left (green box), in the absence of fictive swimming episodes ("non-bout period"), different Purkinje cells show, respectively, a CS-induced i) long SS pause, ii) short SS pause with rebound increase, iii) no change in SS, iv) short SS increase, and finally a v) long SS increase. These relationships change in most cells during fictive bout periods ("bout period", changes highlighted by green arrowheads). Middle (blue box), these relationships are similar across all sensory contexts when the fish is not swimming, regardless of whether the CS occurs during the preferred sensory stimulus driving complex spikes in that cell or at all other non-swimming periods during the trial. Right (grey box), the modulation of simple spike rates by spontaneous CS (blank trials) is consistent with the relationship in all other non-bout contexts. Vertical scale bar indicates the rate conversion for 0.2 spikes / 10 ms bin (20 Hz). e) The mean normalized simple spike rates (calculated from 10 ms bins) for all Purkinje cells centered on the occurrence of a complex spike during a fictive bout minus those occurring at any other point (green markers, mean ± SEM; N=51 cells). The

simple spike rates centered on the occurrence of a complex spike during all sensory stimuli minus those occurring during blank trials are also shown (grey markers, mean ± SEM; N=53 cells; note that all complex spikes that occurred during a fictive bout were excluded from this latter analysis). Cells for which there were less than ten complex spikes for any condition were excluded from analysis. The dashed black line indicates zero difference between conditions. Inset, the window around complex spike onset shown on an expanded timescale. Asterisks indicate $p<0.05$ for motor minus nonmotor conditions (green markers) as computed by the Wilcoxon signed rank test. There are no significant differences in this period between sensory minus blank conditions. f) Heat maps are shown for individual Purkinje cell binned simple spike counts over the three different 50 ms periods as indicated in e). Complex-spike triggered simple spike counts are separated for each cell for those complex spikes occurring during a fictive bout (left column of heatmaps, outlined in green) or at any other time (right column of heatmaps, outlined in black).

Motor context alters the relationship between complex spike and simple spike activity

It is well-established that the occurrence of a complex spike can alter simple spike activity in a Purkinje cell both acutely and across longer timescales (De Zeeuw et al., 2011). On a short timescale, complex spikes typically cause a brief pause of tens of milliseconds in simple spike firing that can be followed by an increase or decrease in simple spikes lasting hundreds of milliseconds. The particular complex spike-triggered change in simple spiking is robust for a given Purkinje cell but varies considerably across cells (Zhou et al., 2014, 2015; Xiao et al., 2014). Similar to previous findings, we observed heterogeneity in the relationship between complex and simple spikes across Purkinje cell recordings (Figure 5c). At the most extreme end, we observed complex spike-induced pauses or increases in simple spike rates that took several hundred milliseconds to return to baseline. These pauses or increases in simple spiking may be attributable to a toggling action of the complex spike to shift the Purkinje cell between “up” and “down” states (Loewenstein et al., 2005; Sengupta & Thirumalai, 2015). Several cells had brief pauses (tens of milliseconds) following a complex spike which left simple spikes otherwise unchanged, whereas others showed a brief increase in simple spike firing. Previous studies have revealed that the modulation of simple spike firing by a complex spike is related to the cell’s location within the cerebellum (Zhou et al. 2014, 2015). We did not, however, observe any clear spatial organization of the complex spike-simple spike relationship in this dataset (Figure 5c).

The current behavioral state of the animal should provide important contextual information for cerebellar circuits, therefore we hypothesized that the modulation of simple spikes by a complex spike might be altered in different sensory and motor contexts. In periods during which the fish was at rest (no fictive swimming), the relationship between complex spikes and simple spike firing rates was consistent whether or not visual stimuli were being presented (Figure 5d, “non-motor” versus “blank trials”). When the fish was performing a fictive swimming bout however, the effect of a

complex spike on simple spike output appeared diminished (Figure 5d, “non-motor” versus “motor”), which was not the case for complex spikes occurring during a cell’s preferred complex spike sensory stimulus versus those occurring during all other periods (Figure 5d, “pref. sensory” versus “all other periods”).

The unique effect of motor context on this relationship is likely related to the finding that many Purkinje cells have simple spike rates that are strongly excited by motor activity (Figure 4c-e), therefore a complex spike stochastically occurring during a bout would be faced with simple spikes rates that are significantly higher than baseline. Upon closer examination of the temporal window around the occurrence of a complex spike, we observed that the acute effect of a complex spike to modulate simple spike rates was identical between motor and non-motor periods for only a 50 millisecond period following the complex spike, after which time simple spiking returned to high levels correlated with ongoing behavior (Figure 5e,f). This temporal window was the same across cells regardless of whether the baseline modulation by a complex spike was to pause or facilitate simple spike firing. These findings suggest that the acute effect of a complex spike to change simple spike output in a Purkinje cell is temporally restricted by the behavioral state of the animal and that plasticity mechanisms relying on coincident complex spike and simple spike activity will have a unique dependence on motor context (see discussion).

DISCUSSION

In this study, we have characterized the spatial integration of sensory and motor information in cerebellar Purkinje cells from excitatory input streams during simple visuomotor behaviors in the larval zebrafish. We show that Purkinje cells fall into anatomically clustered regions that are functionally defined by complex spike responses that convey mostly sensory information. On the other hand, simple spikes convey mostly motor-related information about tail and eye movement. Information arriving via these two streams in a given region likely represent a behavioral module whose neural computations are used to guide sensorimotor integration and motor learning in the cerebellum.

Complex spikes encode sensory and not motor information

Our results show that that majority of Purkinje cells across the cerebellum encode sensory and not motor information in their complex spike activity. We observed a strikingly discrete and complete

classification of nearly all Purkinje cells (>90%) for a specific visual complex spike response whose sensory nature was clearly distinguishable from motor-related signals of eye and tail behavior. These visually-evoked responses may signal unexpected events or "negative sensory events to be avoided" such as retinal slip (Lang et al., 2017). This is not necessarily a classical error signal (Ito, 2013) because stimulus-evoked complex spikes are equally prominent in paralyzed fish as in experiments where the eyes and tail are free and track the stimulus. Furthermore, many complex spikes are robustly elicited by sensory stimuli that do not drive behavior, such as reverse motion or luminance changes. In cases when complex spikes are driven by the onset of directional translational motion, they tend to precede behavior but do not predict it, since for example forward translational movement elicits variable bouts of swimming and not across all trials, yet the sensory complex spike response does not change. These results argue against an interpretation that these complex spikes carry predictive motor signals. In our experiments, complex spikes are consistently elicited by visual stimuli, across many trials and many hours. It remains to be seen how robust these responses are over longer timescales, as previous work has suggested the complex spike response to a sensory stimulus is driven by its novelty and therefore subject to habituation with repeated exposure across many days (Ohmae & Medina, 2015). Nonetheless, the complex spike responses we observed are clearly selective for certain visual features and not encoding novel stimuli in general. The current findings furthermore suggest that there is limited multiplexing of visual features or of visual and motor information in these complex spike responses (Kitazawa et al., 1998), therefore our interpretation is that complex spikes convey rather straightforward sensory signals in this experimental context. Additional work is needed to determine how the complex spike responses to other sensory modalities map onto these functional regions and within individual Purkinje cells.

Anatomical organization of cerebellar regions

The three distinct regions formed along the rostrocaudal axis of the larval zebrafish cerebellum we define here based on distinct Purkinje cells sensory complex spike phenotypes to visual stimuli should receive specific inputs from the inferior olive (Figure 6; Ozol et al., 1999). Ongoing work characterizing the physiology and anatomy of inferior olive neurons and their climbing fibers (unpublished observations) supports this regional characterization and together with studies of Purkinje cell output to eurydendroid cells will further our understanding of these anatomical regions. Differences in developmental timing are known to contribute to the formation of a topographic functional map in the cerebellum across species (Hashimoto & Hibi, 2012). In zebrafish, Purkinje cell development occurs in waves that map onto the same regions we describe here, beginning

with a large rostromedial cluster and a smaller, caudolateral cluster and later filling in the central region to form a continuous layer (Hamling et al., 2015). Regional differences in cytoarchitecture and patterns of molecular markers such as zebrin have also been useful for identifying related Purkinje cells into groups in the mammalian cerebellum (see Cerminara et al., 2015 for review). Although in larval zebrafish all Purkinje cells are zebrin-positive (Bae et al., 2009), many other genes are expressed in restricted patterns in the zebrafish (Takeuchi et al., 2017) and mammalian cerebellum (Hawkes, 2014) that could help understand the subdivision of Purkinje cells into clearly-defined regions and subregions across the cerebellum.

Regional functionality of the zebrafish and mammalian cerebellum

The anatomical organization of the cerebellum is thought to impart distinct functional roles onto cerebellar regions, such that groups of Purkinje cells process information relating to different sensorimotor behaviors (Witter & de Zeeuw, 2015). Although we only probed one sensory modality to drive behavior, zebrafish are highly visual animals that perform robust visuomotor behaviors at the larval stage, including prey capture, optokinetic and optomotor responses, and associative learning with a conditioned visual stimulus (Nicola & Easter, 1996; Budick & O'Malley, 2000; Aizenberg & Schuman, 2011; Harmon et al., 2017). Visual information is therefore a highly salient sensory modality at this age and in accordance with this strong ethological relevance we find that the complex spike sensory responses to visual stimuli provide an overarching organization of the Purkinje cell layer into behavioral modules (Figure 6).

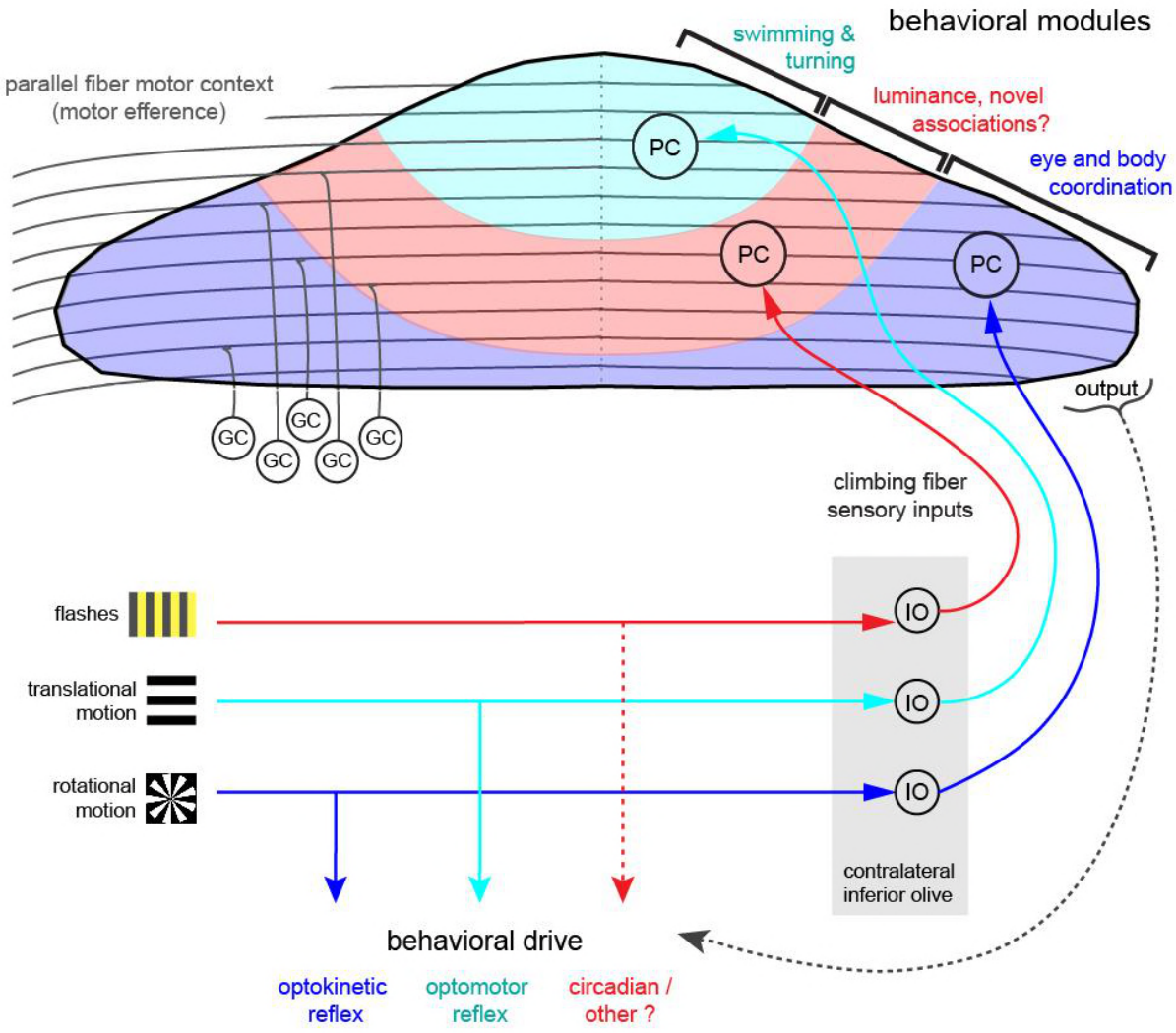

Figure 6. Schematic model for the functional organization of the larval zebrafish cerebellum

Granule cells (GCs) send long parallel fibers (grey lines) that contact Purkinje cells (PCs) across the cerebellum and broadly relay motor efference copies of locomotor activity (swimming). Sensory information relating to different visual features are sent by climbing fibers of inferior olive neurons (IO) to stereotyped regions of the contralateral Purkinje cell layer. These visual stimuli contribute to several reflexive behaviors; rotational motion drives the optokinetic reflex of the eyes, translational forward motion drives the optomotor swimming reflex while others, such as luminance, may drive behavior over longer (e.g. circadian) timescales. We believe that the three distinct functional regions in the zebrafish cerebellum defined by Purkinje cell complex spike sensory responses that encode these different visual features represent behavioral modules. Information about the onset of translational motion in different directions is preferentially sent to Purkinje cells in the rostromedial region of the cerebellum (cyan) and would be important for coordinating turning and swimming, while information about the direction and velocity of rotational motion as would be needed for coordinating eye and body movements is sent to the caudolateral region (blue). The intermediate region receives information about luminance (red) and may provide a substrate for novel, learned sensorimotor associations.

Transient changes in the direction of translational motion, encoded by the rostromedial cerebellum, convey information critical for driving swimming and turning behaviors in the larval zebrafish, or in the case of visual reafference, for evaluating the success of a directed behavior. This population of Purkinje cells whose complex spikes encode directionally-selective motion onset are reminiscent of the directionally-tuned Purkinje cells in the oculomotor vermis of posterior lobes VI and VII in primates (Soetedjo & Fuchs, 2006; Herzfeld et al., 2015). In the caudolateral region we find Purkinje cells with strong complex spike responses to unidirectional rotational motion and axons that project primarily to the octaval nuclei in zebrafish (Matsui et al., 2014). These Purkinje cells fire complex spikes during contraversive (temporal to nasal, with respect to the Purkinje cell) movement in the contralateral visual field. This caudal region is likely the vestibulocerebellum, homologous to the mammalian flocculonodular lobe where Purkinje cells receive climbing fiber input conveying information about ongoing, opposing directional visual and rotational head motion that is used for vestibulo-ocular coordination (Simpson & Alley, 1974; Ito, 1982). Notably, these zebrafish vestibulocerebellar Purkinje cells show complex spike responses not only to rotational but also to translational moving fields, which is not seen in mammals but has been observed in pigeons (Wylie & Frost, 1991). This finding may relate to the additional complexity of optic flow that arises during navigation in a three-dimensional world for birds and fish.

We furthermore observe that Purkinje cells in the caudolateral region have spontaneous complex spike rates an order of magnitude higher than those in the rostromedial region described above and show sustained high complex spike firing in response to their preferred stimulus. This could allow for increased temporal precision in order to generate fast and precise firing patterns as would be required when generating sensorimotor associations or coordinating smooth movements (Porrill et al., 2013, Suvrathan et al., 2016). The computation itself may in fact be different since complex spikes in this region could use conventional rate coding to encode the speed and direction of ongoing, slow movements of the visual field during behavior, as proposed by Simpson et al. (1996) based on observations in the mammalian flocculonodular lobe across species. These findings challenge the widely-held assumption that the computations being performed across the cerebellum all follow the same rules and that the occurrence of a discrete event, rather than information about an ongoing event, is transmitted by complex spikes.

Sensory complex spike coding of luminance in the intermediate region of the zebrafish cerebellum shows significant heterogeneity across cells which may reflect involvement in different behaviors modulated by luminance. At greater magnitudes, sudden decreases in luminance induce re-

orienting navigational turns (Burgess & Granato, 2007) or escapes (Temizer et al., 2015) in zebrafish larvae and transient startle responses in the adult (Easter & Nicola, 1996), the latter two representing likely predator avoidance responses. Luminance has also been found to increase spontaneous locomotor activity in the larva over longer timescales, which could be used as a cue to regulate circadian rhythms and motivate feeding and exploratory behavior in the daytime (Burgess & Granato, 2007). Purkinje cells in this central region are born slightly later in development (Hamling et al., 2015), suggesting that this region could also be suited for flexible or learned behaviors. Recent work in zebrafish revealed that Purkinje cells in this intermediate region of the cerebellum preferentially acquired complex spike responses to a conditioned light stimulus (Harmon et al., 2017), supporting the idea that this region could preferentially contribute to learned sensorimotor associations. This region may be similar to areas in the central zone (posterior lobes VI and VII) of the cerebellum in mammals, which support a wide range of behavioral functions (Koziol et al., 2015; Stoodley et al., 2012). The function and organization of the zebrafish cerebellum across regions may furthermore change to reflect an increasing complexity and repertoire of behaviors at later developmental stages.

Motor efference copies in the cerebellum

Our population-wide imaging and extensive electrophysiological recordings show that Purkinje cells across the cerebellum encode the current behavioral state (motor context) of the animal through a pronounced increase in simple spikes during locomotor behaviors. We observed strong swim-related signals in granule cells and Purkinje cells during both active and fictive swimming, where zebrafish were awake but paralyzed, therefore this activity is more consistent with motor efference copy signals than proprioceptive or lateral line activation. Moreover, we found that simple spike output correlated best with the strength of swimming rather than reporting binary locomotor state, supporting previous findings that motor parameters are linearly coded in the cerebellum (Raymond & Medina, 2018). The increases in simple spike output that we observe are far less heterogeneous than the effects of locomotion on mammalian Purkinje cell simple spike firing (Jelitai et al., 2016; Sauerbrei et al., 2015) and build on previous electrophysiological samplings of Purkinje cell activity that showed increases in membrane depolarization and simple spike output during fictive swimming in zebrafish (Sengupta & Thirumalai, 2015; Scalise et al., 2016). These results suggest that motor efference signals during whole-body locomotion (swimming) drive simple spike output in nearly all cerebellar Purkinje cells in the larval zebrafish. Our additional granule cell population imaging and electrophysiological recordings in zebrafish together with other recordings in zebrafish and mice (Ozden et al., 2012; Powell et al., 2015; Jelitai et al., 2016; Giovannucci et al., 2017; Knogler et al.,

2017; Albergaria et al. 2018) provide strong evidence that the cerebellum broadly encodes intended locomotor output or signals related to it in the input layer (Figure 6). Future work is required to investigate the origin of mossy fibers carrying eye and tail motor efference copies to the zebrafish cerebellum and how these signals are transformed by subsequent processing stages in cerebellar circuits.

Evidence for a forward internal model

The cerebellum has been implicated in internal models of motor control. Simple spikes in Purkinje cells driven by motor efference copies may convey more than just the occurrence of a motor event. In a forward model, the motor efference copy is used to predict the sensory consequences that should result from the movement, i.e. the reafference (Miall et al., 1993). These predictions will also be motor-related, and in fact it is likely that the simple spike activity we observe is a mixture of both (Porrill et al., 2013; Ishikawa et al., 2016). Physiological recordings from granule cells (Ishikawa et al., 2015; Knogler et al., 2017) and other anatomical studies (Huang et al., 2013; Chabrol et al., 2015) show that both motor and sensory signals converge on individual granule cells and may thus provide the substrate for these reafferent signals. As mentioned above, we find that climbing fiber inputs to Purkinje cells primarily encode sensory information. If these do indeed correspond to teaching signals, from a computational perspective, we would expect the contextual information from parallel fibers and the climbing fiber activity to be in the same basis in order to compare the predicted and actual sensory consequences of the motor command (Porrill et al., 2004, 2013; Dean et al., 2002). This interpretation agrees with the notion that the cerebellum generates rapid predictions about state estimation and expected sensory feedback through a forward model (Wolpert et al., 1998). This is in contrast to models of eyelid conditioning that resemble inverse models of motor control, where the sensory context of the conditioned tone stimulus is conveyed via mossy fibers and granule cells while climbing fibers encode motor errors (Steinmetz et al., 1986, 1987). Although it is unreasonable to expect a simple straightforward mapping between these internal models and the olivo-cerebellar system, we believe that this framework constitutes a valuable tool to understand cerebellar function and future work is needed to flesh out this analogy.

Complex spike - simple spike relationships

Internal models need to be adjusted during development, experience, and learning, so that the behaviors being performed by an animal can adapt to suit a changing environment or context. Classical theories of supervised cerebellar learning predict that the coincident activation of a climbing fiber input and parallel fiber synapses drives long-term depression at the active parallel

fiber to Purkinje cell synapses, leading to motor learning (Ito, 2001; but see Bouvier et al., 2017). Synaptic plasticity mechanisms both at other synapses and involving other cerebellar neurons (e.g. interneurons) are also likely to contribute (see Gao et al., 2012 for review). We propose that motor efference signals during swimming and eye movement are broadcasted widely across the cerebellum to Purkinje cells because these are the most relevant signals not only for coordinating ongoing behaviors but also for driving plasticity. The enrichment of motor-related activity across the entire cerebellum allows for a large substrate to support novel associations between motor behaviors and the sensory information carried by regionally-specially climbing fiber input.

Motor activity not only dominates the output from Purkinje cells but also changes how complex spikes and simple spikes interact. During non-locomotor periods, we observe that the temporal effects of complex spikes on simple spike output, encapsulated by the complex spike-triggered simple spike averages, are heterogeneous across Purkinje cells, such that in some cells a complex spike consistently increases or pauses simple spiking for several hundreds of milliseconds. Under motor-driven conditions of high simple spike rates, however, a complex spike now resets simple spike activity for only a brief (<50 ms) window in all Purkinje cells before simple spikes return to their previous high rate. A complex spike arriving during motor activity is therefore special not only because its acute effect to control simple spike output becomes temporally limited, but because in most Purkinje cells parallel fiber inputs carrying motor information will be highly coincidently active, and therefore incoming complex spikes should drive significant plasticity. This may be interpreted as the fact that a complex spike occurring during a motor event may be serving to bring the simple spike firing rate back to baseline during a very precise time window.

The specific features of the three functional cerebellar regions we define here have additional implications for plasticity. The elevated spontaneous complex spike rate we find in the vestibulocerebellum suggests an increased probability of complex spikes stochastically arriving during motor behaviors, which could drive acute variations in behavior as a potential means to explore motor parameter space and behavioral optimization (Lisberger & Medina, 2015). The temporal patterning of luminance-evoked complex spikes we observe in the central region, which may arise from phase differences in electrically-coupled inferior olive networks, could drive plasticity in neighboring cells at slightly different time intervals as required for a learned motor sequence (Jacobson et al., 2008). A detailed examination of synaptic plasticity mechanisms (Ito, 2001) and timing rules (Suvrathan et al., 2016) in the zebrafish cerebellum is needed to understand the impact of motor context at the cellular level.

Outlook

Our results reveal a spatial organization of sensory encoding in the Purkinje cell population into three rostrocaudal functional regions receiving different climbing fiber inputs. These regions are each involved in processing visual information relating to distinct motor behaviors. Broad excitation from granule cells is layered on these regions during locomotor activity as a contextual signal. We believe that the system of granule cells and Purkinje cells together thus forms the substrate of internal models, which can be updated by climbing fiber input. These and other recent findings (Matsui et al., 2014; Harmon et al., 2017) provide a promising outlook for using the zebrafish as a model organism to understand Purkinje cell physiology in the context of cerebellar modules modulating innate and learned motor behaviors.

MATERIALS AND METHODS

Experimental Model and Subject Details

Zebrafish (*Danio rerio*) were maintained at 28˚C on a 14hr light/10hr dark cycle using standard protocols. All animal procedures were performed in accordance with approved protocols set by the Max Planck Society and the Regierung von Oberbayern. All experiments were performed using larvae at 6-8 dpf of as yet undetermined sex.

To label Purkinje cells specifically, we made use of the aldoca promoter and the carbonic anhydrase 8 (ca8) enhancer element as published previously (Takeuchi et al., 2014, Matsui et al., 2014). For electrophysiological recordings in Purkinje cells, aldoca:GFF;mn7GFF;UAS:GFP fish were used (Takeuchi et al., 2014; Asakawa et al., 2008, 2013), with Tg(gSAIzGFFM765B); UAS:GFP and Tg(gSAG6A); UAS:GFP fish additionally used for granule cell recordings (Takeuchi et al., 2014). For calcium imaging experiments with granule cells, Tg(gSA2AzGFF152B); UAS:GCaMP6s fish were used (Takeuchi et al., 2015; Thiele et al. 2014). For calcium imaging experiments in Purkinje cells, we cloned GCaMP6s (Chen et al., 2013) downstream of the ca8 enhancer with an E1b minimal promoter referred hereafter as PC:GCaMP6s. We injected PC:GCaMP6s together with tol2 mRNA in one cell stage embryos (25 ng/µl each), screened at 6 dpf for expression in the cerebellum, and raised strong positive fish to adulthood. Positive F1 progeny were used for all imaging experiments. For simultaneous electrophysiological and imaging experiments, we injected PC:GCaMP6s without tol2 mRNA to achieve sparse, single-cell labelling. For anatomical experiments, we created a construct harboring a bright GFP variant mClover3 (Bajar et al., 2016) tagged with a membrane targeting signal (Fyn). This construct is termed PC:Fyn-mClover3. Injections were done as described for sparse GCaMP6s labelling in fish expressing aldoca:gap43-mCherry to allow registration across fish. For optogenetics experiments we cloned channelrhodopsin 2 (ChR2) harboring the H134R mutation (Nagel et al., 2005) that has larger photocurrents downstream of the ca8 enhancer element and fused it to tagRFP (PC:ChR2(H134R)-tagRFP) to avoid ChR2-activation while screening and approaching the cell. Sparse labelling was achieved by injecting PC:ChR2(H134R)-tagRFP with tol2 mRNA in one cell stage embryos.

Functional population imaging

Volumetric functional imaging in the larval zebrafish cerebellum was performed as previously described in Knogler et al., 2017. Briefly. 6-8 dpf nacre (*mitfa* -/-) transgenic zebrafish larvae with

GCaMP6s expressed in Purkinje cells were embedded in 1.5-2.5% agarose prior to imaging. Neural activity was recorded with a custom-built two-photon microscope. A Ti- Sapphire laser (Spectra Physics Mai Tai) tuned to 905 nm was used for excitation. Larval brains were systematically imaged while presenting visual stimuli (see below) at 60 frames per second using a Telefunken microprojector controlled by custom Python software and filtered (Kodak Wratten No.25) to allow for simultaneous imaging and visual stimulation. We acquired the total cerebellar volume by sampling each plane at ~ 5 Hz. After all stimuli were shown in one plane, the focal plane was shifted ventrally by 1 µm and the process was repeated. Tail and eye movement was tracked throughout with 850nm infrared illumination and customized, automated tracking software. Behavior was imaged at up to 200 frames per second using an infrared-sensitive charge-coupled device camera (Pike F032B, Allied Vision Technologies) and custom written software in Python.

Single cell Purkinje cell imaging

Sparse labelled Purkinje cells expressing GCaMP6s were used to perform two-photon imaging as described above to identify any signal compartmentalization (Figure S1). Visual stimuli consisting of reverse and forward moving gratings were probed to evoke signals in Purkinje cells. For five Purkinje cells across three fish, ROIs for soma and parts of the dendrite were drawn manually and Calcium traces were extracted using custom-written software in Python. The most distal dendritic ROI was correlated with somatic ROI to determine the correlation coefficient for each cell.

Visual stimuli

For functional imaging experiments, trials were presented that consisted of the following stimuli, in non-randomized order: Black and white whole-field gratings were presented with motion in the forward direction at slow, medium, and fast speeds (3,10, and 30 mm/s, respectively), for five seconds each with a pause of five seconds between stimuli, followed by reverse, leftward, and rightward moving gratings of the same duration and at medium speed. Grating remained static between stimuli. Black and white windmill patterns were rotated at 0.2 Hz with changing velocity that followed a sine function. Windmill patterns were presented across the whole field as well as for each half of the visual field. Flashes covered the whole visual field and switched between maximum luminance and darkness. For electrophysiological recordings, stimuli were similar as for functional imaging with the exception that the stimulus set had shorter pauses between stimuli and that fewer repetitions of the rotating windmill stimulus were presented. Blank trials consisting of static gratings were also interspersed with stimuli trials to obtain baseline responses. For one

experiment (Figure S3g) the fish was also presented with a series of whole-field black or white flashes of various durations (50 - 5000 ms) against a baseline intermediate luminance.

Imaging analysis

Image analysis was performed with MATLAB (MathWorks) and Python similar to Knogler et al. (2017). Python analysis used scikit-learn and scikit-image (Pedregosa et al., 2011, van der Walt et al., 2014). Volumetrically-acquired 2-photon data was aligned first within a plane then across planes to ensure that stacks were aligned to each other with subpixel precision. Any experiments during which the fish drifted significantly in z were stopped and the data discarded. The boundary of the cerebellum was manually masked to remove external signals such as skin autofluoresence.

Tail activity during imaging experiments was processed to yield a vigor measurement that was greater than zero when the fish is moving. Independent left and right eye position and velocity were obtained from eye tracking data. Motor regressors for each imaging plane were created from these behavioral parameters. Sensory regressors were the same across trials and built using features including the onset, duration, direction, and velocity of moving stimuli as well as luminance. All regressors were convolved with a GCaMP kernel (tau=1600ms). We performed voxel-wise multi-linear regression with normalized convolved regressors and present here mean z-projections of the regressor coefficients. Purkinje cell maps show a representative fish. Granule cell maps are means of seven morphed fish and were manually masked either for parallel fibres and granule cell somata somata to show potential differences in the signal topography. To further dissociate motor and sensory responses for sensory stimuli that strongly drive a particular behavior (translational motion and swimming, or rotational motion and left/right eye velocities), we used a maximum intensity projection of respective sensory and motor regressor maps and colored a pixel depending on whether sensory (magenta) or motor (green) regressors explain this pixel better with a given minimum distance. Differences that are below that minimum distance or are uncorrelated are colored white. Example Purkinje cell activity traces used in Figure 1 were extracted using automated algorithms based on local correlations between pixels (see Portugues et al., 2014 for details).

In order to understand activity as a whole as opposed to in relation with particular regressors, we performed PCA on the vector of correlations with all regressors for all automatically segmented ROIs and all fish. This correlation vector representation was clustered in the PC space in 10

clusters using kmeans. This number was chosen because 10 PCs already explained ~90% of the variance. All voxels were then colored in according to the cluster they belonged to.

The anatomical clustering and stereotypy indices were calculated as follows. For the anatomical clustering index, the average distance between ROIs of the same cluster within a fish was compared against the average distance between an ROI from that cluster and a randomly chosen ROI from that fish. The inverse ratio of these two quantities is the anatomical clustering index. The stereotypy index is computed similarly. In this case, the average distance between an ROI from a particular cluster and fish and other ROIs from that same cluster but other fish is compared against the distance between an ROI from that same cluster and fish and other ROIs from other clusters and fish. Again, the inverse ratio of these two quantities is the stereotypy index. To summarize, the index is a comparison of average distance within a condition to average distance without the restraint of that condition.

Electrophysiological neural recordings

Cell-attached electrophysiological recordings were performed in 6-8 dpf zebrafish as previously described (Knogler et al., 2017) using an Axopatch Multiclamp 700B amplifier, a Digidata series 1550 Digitizer, and pClamp 9 software (Axon Instruments, Molecular Devices). Data were acquired at 8.3 kHz using Clampex 10.2. Wild-type or transgenic zebrafish larvae with GFP-positive Purkinje cells and motor neurons were used for most recordings (see subject details above).

Larvae were paralyzed in bath-applied buffered 1 mg/ml alpha-bungarotoxin (Cayman Scientific, Concord, CA) and embedded in 1.5% low melting point agarose in a 35mm petri dish. External solution was composed of Evans solution (134 mM NaCl, 2.9 mM KCl, 2.1 mM CaCl2, 1.2 mM MgCl2 , 10 mM glucose, 10 mM HEPES, pH 7.8 with NaOH). Electrodes for neuron recordings (6-12 MΩ) were pulled from thick-walled borosilicate glass with filament and were filled with the following intracellular solution (in mM): 105 D-gluconic acid, 16 KCl, 2 MgCl2, 10 HEPES, and 10 EGTA, adjusted to pH 7.2, 290 mOsm (Drapeau et al., 1999). Sulforhodamine B (0.1%) was included in the intracellular solution to visualize the electrode. The skin overlying the cerebellum was carefully removed with a glass electrode prior to recording. Post-recording fluorescent images of GFP-positive Purkinje cells and the recording electrode (visualized with an RFP filter) as well as bright-field images to confirm cell identity and map somatic location were acquired with an epifluorescent ThorLabs camera controlled by Micromanager.

Electrophysiological data were analyzed offline with Clampfit 10.2 software (Molecular Devices) and Matlab (Mathworks, Natick MA). Cell-attached traces were high-pass filtered at 1-10 Hz and complex spikes and simple spike were automatically extracted by setting a threshold for each type of spike in that recording. A 2.5 ms period was blanked following each complex spike so that the complex spike waveform did not cross the simple spike threshold. Baseline firing rates were calculated from blank trials where no visual stimuli were presented or from the two second period at the beginning of each trial prior to the first stimulus onset if no blanks were obtained.

For experiments with simultaneous calcium imaging, stochastically-labeled single Purkinje cells expressing GCaMP6s were recorded with an epifluorescent backlit-CMOS camera (Photometrix Prime 95B) at 11.5 fps controlled by Micromanager and triggered by pClamp software during electrophysiological recordings. No visual stimuli were shown in these experiments. Fluorescent Purkinje cell activity was processed by manual ROI extraction. Extracted complex spike and simple spike rates from simultaneous electrophysiology traces were convolved with a GCaMP6 kernel for comparison with the fluorescent signal.

For electrophysiological recordings in the semi-paralyzed animal, larval zebrafish were embedded in 2% low-melting point agarose and injected with 0.5 mg/ml alpha-bungarotoxin in the caudal tip of the tail. This method reduces the trunk contractions during swimming but preserved full eye movement. The agarose around the eyes was removed and the fish was lit from below with 850nm infrared illumination to allow for good image contrast of the eyes. Eye movement was recorded during simultaneous electrophysiological recordings and tracked offline with customized, automated software to extract independent trajectories for each eye.

Ventral root recordings and analysis

To obtain extracellular ventral root recordings, a thin-walled borosilicate glass electrode with a large opening (approximately a quarter of the width of a somite) was first used to remove a small section of skin overlying the horizontal myotomes of the spinal cord around the fifth spinal somite. The electrode was then cleared with positive pressure and positioned over the terminals of the ventral root with gentle suction to ensure good signal to noise.

Motor activity was extracted as a moving standard deviation of the ventral root trace. A threshold was then applied to identify ventral root activity that would correspond to motor output on the side of the animal ipsilateral to the recording electrode. To extract a binarized trace of swimming bouts,

ventral root activity separated by an interval of less than 100 ms was considered to be part of the same bout. The vigor trace was median filtered to extrapolate vigor information across the entire bout. Peaks in the lag of the autocorrelation analysis of the thresholded, binarized signal was used to extract fictive swim frequency.

Electrophysiology analyses with multilinear regression

Purkinje cell complex spikes and simple spikes were concatenated across trials and filtered over 20 ms bins to extract firing rates from electrophysiological recordings. Motor regressors for each cell were calculated using the concatenated extracted bout information including bout onset, offset, duration, and vigor. Sensory regressors for each trial were the same for all cells and were created using features including the onset, duration, direction, and velocity of moving stimuli as well as luminance (see Figure S2 for full regressor list). Least-squares ridge regression was then used to determine the coefficient weights of the matrix of sensory and motor regressors concatenated across all recorded trials for each cell with its complex spike and simple spike firing rates. Alpha was 0.2 therefore the elastic net regression approaches ridge regression. Changing the alpha parameter to move closer to an elastic net optimization did not significantly alter the main regressor weights but rather assigned some extremely small (nearly zero) weights to other regressors. Lambda, a regularization parameter, was set to initial values of 0.9 to calculate regressor coefficient weights. The number of nonzero coefficient weights were calculated and the regression was rerun with a Lambda value in decreasing increments of 0.1 until at least three nonzero weights were present for both simple spike and complex spike rates. Once again, initializing parameters with a lower Lambda value did not significantly alter the distribution of coefficient weights. The same procedure was used to obtain granule cell coefficient weights.

For detailed analysis of the different classes of sensory complex spike responses (Figure 2), we included for analyses all Purkinje cells for which that regressor coefficient weight was significant. To determine which Purkinje cells showed significant responses to luminance, we used autocorrelation analyses of complex spike rates during whole-field flashes only and assessed significance using the Ljung-Box Q-test.

Purkinje cell morphology

Sparsely labelled Purkinje cells were imaged using a 20x water immersion objective with 1 NA (Zeiss) on a confocal microscope (LSM 700, Carl Zeiss, Germany). High resolution stacks of Purkinje cells were deconvolved using Richardson-Lucy algorithm and artifacts were removed

manually. Purkinje cell axonal projections were traced using NeuTube (Feng et al., 2014) and the Simple Neurite Tracer plugin for FIJI (Longair et al., 2011). SWC files were converted to line stacks and post-processed using custom written software in Python. Individual axonal projections were morphed together using aldoca:gap43-mCherry as reference and CMTK as morphing tool (Rohlfing & Maurer, 2003). Dendritic planarity by performing principal component analysis on binarized dendritic morphologies. The ratio of the third principal component to the second was used to determine planarity (planar dendrites have ratios approaching 0, whereas nonplanar dendrites have ratios approaching 1).

Quantification and Statistical Analysis

Data were analyzed in MATLAB and Python with custom software.

Baseline complex spike firing rates for groups of Purkinje cells sorted by complex spike phenotype were compared by one-way ANOVA, followed by pairwise *post hoc* analyses using Bonferroni post hoc correction. The nonparametric Wilcoxon signed rank test was used on paired nonparametric datasets. Details of statistical analyses are found in the text and figure legends.

Data/resource sharing

Further information and requests for data, resources, and reagents should be directed to Ruben Portugues (rportugues@neuro.mpg.de).

Acknowledgements

We thank Reinhard Köster for kindly providing the ca8 backbone used for transgenic line development. We thank Herwig Baier for providing mn7GFF;UAS:GFP and UAS:GCaMP6s fish**.** We thank Oliver Griesbeck for use of a Photometrics Prime 95B camera. We thank David Herzfeld and Vilim Štih for helpful comments on the manuscript. LDK was funded by the Alexander von Humboldt Foundation, the Carl von Siemens Foundation, the Fonds de recherche du Québec - Santé, and the Max Planck Gesellschaft (MPG). AMK was funded by the International Max Planck Research School for Life Sciences (IMPRS-LS), a Joachim-Herz fellowship, and the MPG. RP was funded by the MPG. This research was also partly funded by the DFG (Deutsche Forschungsgemeinschaft - German Research Foundation) through grant PO 2105/2-1. LDK would like to dedicate this paper to the memory of her colleague and friend, Dr. Sean E. Low.

Author Contributions

LDK and RP designed the study and experiments. LDK carried out electrophysiology experiments and imaging experiments. AMK created transgenic lines and carried out imaging experiments. LDK, AMK, and RP performed data analysis. LDK and RP wrote the manuscript with help from AMK.

Competing Interests

The authors declare no competing interests.

REFERENCES

Ahrens, M.B., Li, J.M., Orger, M.B., Robson, D.N., Schier, A.F., Engert, F., Portugues, R., 2012. Brain-wide neuronal dynamics during motor adaptation in zebrafish. Nature 485, 471–7. doi:10.1038/nature11057

Aizenberg, M., Schuman, E.M., 2011. Cerebellar-dependent learning in larval zebrafish. J. Neurosci. 31, 8708–8712. doi:10.1523/JNEUROSCI.6565-10.2011

Albergaria, C., Silva, N.T., Pritchett, D.L., Carey, M.R., 2018. Locomotor activity modulates associative learning in mouse cerebellum. Nat. Neurosci. 21, 725–735. doi:10.1038/s41593-018-0129-x

Albus, J.S., 1971. A theory of cerebellar function. Math. Biosci. 10, 25–61. doi:10.1016/0025-5564(71)90051-4

Apps, R., 1999. Movement-related gating of climbing fibre input to cerebellar cortical zones. Prog. Neurobiol. 57, 537–562. doi:10.1016/S0301-0082(98)00068-9

Apps, R., Garwicz, M., 2005. Anatomical and physiological foundations of cerebellar information processing. Nat. Rev. Neurosci. 6, 297–311. doi:10.1038/nrn1646

Apps, R., Hawkes, R., 2009. Cerebellar cortical organization: a one-map hypothesis. Nat. Rev. Neurosci. 10, 670–681. doi:10.1038/nrn2698

Arenz, A., Bracey, E.F., Margrie, T.W., 2009. Sensory representations in cerebellar granule cells. Curr. Opin. Neurobiol. 19, 445–451. doi:10.1016/j.conb.2009.07.003

Asakawa, K., Abe, G., Kawakami, K., 2013. Cellular dissection of the spinal cord motor column by BAC transgenesis and gene trapping in zebrafish. Front. Neural Circuits 7, 1–14. doi:10.3389/fncir.2013.00100

Asakawa, K., Suster, M.L., Mizusawa, K., Nagayoshi, S., Kotani, T., Urasaki, A., Kishimoto, Y., Hibi, M., Kawakami, K., 2008. Genetic dissection of neural circuits by Tol2 transposon-mediated Gal4 gene and enhancer trapping in zebrafish. Proc. Natl. Acad. Sci. U. S. A. 105, 1255–1260.

Badura, A., Schonewille, M., Voges, K., Galliano, E., Renier, N., Gao, Z., Witter, L., Hoebeek, F.E., Chédotal, A., DeZeeuw, C.I., 2013. Climbing fiber input shapes reciprocity of purkinje cell firing. Neuron 78, 700–713. doi:10.1016/j.neuron.2013.03.018

Bae, Y.K., Kani, S., Shimizu, T., Tanabe, K., Nojima, H., Kimura, Y., Higashijima, S.I., Hibi, M., 2009. Anatomy of zebrafish cerebellum and screen for mutations affecting its development. Dev. Biol. 330, 406–426. doi:10.1016/j.ydbio.2009.04.013

Bajar, B.T., Wang, E.S., Lam, A.J., Kim, B.B., Jacobs, C.L., Howe, E.S., Davidson, M.W., Lin, M.Z., Chu, J., 2016. Improving brightness and photostability of green and red fluorescent proteins for live cell imaging and FRET reporting. Sci. Rep. 6, 1–12. doi:10.1038/srep20889

Bouvier, G., Clopath, C., Bimbard, C., Nadal, J.-P., Brunel, N., Hakim, V., Barbour, B., 2017. Cerebellar learning using perturbations. bioRxiv 53785. doi:10.1101/053785

Budick, S.A., O'Malley, D.M., 2000. Locomotor repertoire of the larval zebrafish: swimming, turning and prey capture. J. Exp. Biol. 203, 2565–2579.

Burgess, H.A., Granato, M., 2007. Modulation of locomotor activity in larval zebrafish during light adaptation. J. Exp. Biol. 210, 2526–39. doi:10.1242/jeb.003939

Cerminara, N.L., Apps, R., 2011. Behavioural significance of cerebellar modules. Cerebellum 10, 484–494. doi:10.1007/s12311-010-0209-2

Cerminara, N.L., Lang, E.J., Sillitoe, R. V., Apps, R., 2015. Redefining the cerebellar cortex as an assembly of non-uniform Purkinje cell microcircuits. Nat. Rev. Neurosci. 16, 79–93. doi:10.1038/nrn3886

Chabrol, F.P., Arenz, A., Wiechert, M.T., Margrie, T.W., DiGregorio, D.A., 2015. Synaptic diversity enables temporal coding of coincident multisensory inputs in single neurons. Nat. Neurosci. 18, 718–27. doi:10.1038/nn.3974

Chen, T.-W., Wardill, T.J., Sun, Y., Pulver, S.R., Renninger, S.L., Baohan, A., Schreiter, E.R., Kerr, R.A., Orger, M.B., Jayaraman, V., Looger, L.L., Svoboda, K., Kim, D.S., 2013. Ultrasensitive fluorescent proteins for imaging neuronal activity. Nature 499, 295–300. doi:10.1038/nature12354

De Zeeuw, C.I., Hoebeek, F.E., Bosman, L.W.J., Schonewille, M., Witter, L., Koekkoek, S.K., 2011. Spatiotemporal firing patterns in the cerebellum. Nat. Rev. Neurosci. 12, 327–344. doi:10.1038/nrn3011

Dean, P., Porrill, J., Stone, J. V., 2002. Decorrelation control by the cerebellum achieves oculomotor plant compensation in simulated vestibulo-ocular reflex. Proc. R. Soc. B Biol. Sci. 269, 1895–1904. doi:10.1098/rspb.2002.2103

Dizon, M.J., Khodakhah, K., 2011. The Role of Interneurons in Shaping Purkinje Cell Responses in the Cerebellar Cortex. J. Neurosci. 31, 10463–10473. doi:10.1523/JNEUROSCI.1350-11.2011

Drapeau, P., Ali, D.W., Buss, R.R., Saint-amant, L., 1999. In vivo recording from identifiable neurons of the locomotor network in the developing zebrafish. J. Neurosci. Methods 88, 1–13.

Easter, S.S., Nicola, G.N., 1996. The development of vision in the zebrafish (Danio rerio). Dev. Biol. 180, 646–663. doi:10.1006/dbio.1996.0335

Eccles, J.C., Ito, M., Szentagothai, J., 1967. The cerebellum as a neuronal machine, Book. doi:10.1016/0013-4694(69)90099-6

Feng, L., Zhao, T., Kim, J., 2015. neuTube 1.0: A New Design for Efficient Neuron Reconstruction Software Based on the SWC Format. eNeuro 2. doi:10.1523/ENEURO.0049-14.2014

Gao, Z., Van Beugen, B.J., De Zeeuw, C.I., 2012. Distributed synergistic plasticity and cerebellar learning. Nat. Rev. Neurosci. 13, 619–635. doi:10.1038/nrn3312

Gibson, A.R., Horn, K.M., Pong, M., 2002. Inhibitory Control of Olivary Discharge. Ann. N. Y. Acad. Sci. 978, 219–231. doi:10.1111/j.1749-6632.2002.tb07569.x

Giovannucci, A., Badura, A., Deverett, B., Najafi, F., Pereira, T.D., Gao, Z., Ozden, I., Kloth, A.D., Pnevmatikakis, E., Paninski, L., Zeeuw, C.I. De, Medina, J.F., Wang, S.S.-H., 2017. Cerebellar granule cells acquire a widespread predictive feedback signal during motor learning. Nat. Neurosci. 20, 727–734. doi:10.1038/nn.4531

Hamling, K.R., Tobias, Z.J.C., Weissman, T.., 2015. Mapping the development of cerebellar Purkinje cells in zebrafish. Dev. Neurobiol. 75, 1174–1188. doi:10.1002/dneu.22275

Harmon, T.C., Magaram, U., Mclean, D.L., Raman, I.M., 2017. Distinct responses of Purkinje neurons and roles of simple spikes during associative motor learning in larval zebrafish. Elife 6, 1–26. doi:10.7554/eLife.22537

Harvey, R.J., Napper, R.M.A., 1991. Quantitatives studies on the mammalian cerebellum. Prog. Neurobiol. 36, 437–463. doi:10.1016/0301-0082(91)90012-P

Hashimoto, M., Hibi, M., 2012. Development and evolution of cerebellar neural circuits. Dev. Growth Differ. 54, 373–389. doi:10.1111/j.1440-169X.2012.01348.x

Hawkes, R., 2014. Purkinje cell stripes and long-term depression at the parallel fiber-Purkinje cell synapse. Front. Syst. Neurosci. 8, 1–11. doi:10.3389/fnsys.2014.00041

Herzfeld, D.J., Kojima, Y., Soetedjo, R., Shadmehr, R., 2015. Encoding of action by the Purkinje cells of the cerebellum. Nature 526, 439–442. doi:10.1038/nature15693

Hsieh, J.Y., Papazian, D.M., 2014. Rapid development of Purkinje cell excitability, functional cerebellar circuit, and afferent sensory input to cerebellum in zebrafish. Front. Neural Circuits 8, 1–12. doi:10.3389/fncir.2014.00147

Hsieh, J.-Y., Papazian, D.M., 2018. Extracellular Loose-Patch Recording of Purkinje Cell Activity in Awake Zebrafish and Emergence of Functional Cerebellar Circuit, in: Sillitoe, R. V (Ed.), Extracellular Recording Approaches. Springer New York, New York, NY, pp. 207–224. doi:10.1007/978-1-4939-7549-5_11

Huang, C.C., Sugino, K., Shima, Y., Guo, C., Bai, S., Mensh, B.D., Nelson, S.B., Hantman, A.W., 2013. Convergence of pontine and proprioceptive streams onto multimodal cerebellar granule cells. Elife 2013, 1–17. doi:10.7554/eLife.00400

Ishikawa, T., Shimuta, M., Häusser, M., 2015. Multimodal sensory integration in single cerebellar granule cells in vivo. Elife e12916.

Ishikawa, T., Tomatsu, S., Izawa, J., Kakei, S., 2016. The cerebro-cerebellum: Could it be loci of forward models? Neurosci. Res. 104, 72–79. doi:10.1016/j.neures.2015.12.003

Ito, M., 1972. Neural design of the cerebellar motor control system. Brain Res. 40, 81–84. doi:10.1016/0006-8993(72)90110-2

Ito, M., 1982. Cerebellar control of the vestibulo-ocular reflex--around the flocculus hypothesis. Annu. Rev. Neurosci. 5, 275–297.

Ito, M., 2001. Cerebellar Long-Term Depression: Characterization, Signal Transduction, and Functional Roles. Physiol. Rev. 81, 1143–1196.

Ito, M., 2013. Error detection and representation in the olivo-cerebellar system. Front. Neural Circuits 7, 1. doi:10.3389/fncir.2013.00001

Ito, M., Kano, M., 1982. Long-lasting depression of parallel fiber-Purkinje cell transmission induced by conjunctive stimulation of parallel fibers and climbing fibers in the cerebellar cortex. Neurosci. Lett. 33, 253–258. doi:10.1016/0304-3940(82)90380-9

Jacobson, G. a., Rokni, D., Yarom, Y., 2008. A model of the olivo-cerebellar system as a temporal pattern generator. Trends Neurosci. 31, 617–625. doi:10.1016/j.tins.2008.09.005

Jelitai, M., Puggioni, P., Ishikawa, T., Rinaldi, A., Duguid, I., 2016. Dendritic excitation-inhibition balance shapes cerebellar output during motor behaviour. Nat. Commun. 7, 1–13. doi:10.1038/ncomms13722

Kawato, M., Furukawa, K., Suzuki, R., 1987. A hierarchical neural-network model for control and learning of voluntary movement. Biol. Cybern. 57, 169–185. doi:10.1007/BF00364149

Kennedy, A., Wayne, G., Kaifosh, P., Alviña, K., Abbott, L.F., Sawtell, N.B., 2014. A temporal basis for predicting the sensory consequences of motor commands in an electric fish. Nat. Neurosci. 17, 416–22. doi:10.1038/nn.3650

Kitamura, K., Kano, M., 2013. Dendritic calcium signaling in cerebellar Purkinje cell. Neural Networks 47, 11–17. doi:10.1016/j.neunet.2012.08.001

Kitazawa, S., Kimura, T., Yin, P.B., 1998. Cerebellar complex spikes encode both destinations and errors in arm movements. Nature 392, 494–497. doi:10.1038/33141

Knogler, L.D., Markov, D.A., Dragomir, E.I., Štih, V., Portugues, R., 2017. Sensorimotor Representations in Cerebellar Granule Cells in Larval Zebrafish Are Dense, Spatially

Organized, and Non-temporally Patterned. Curr. Biol. 27, 1288–1302. doi:10.1016/j.cub.2017.03.029

Koziol, L.F., Budding, D., Andreasen, N., D'Arrigo, S., Bulgheroni, S., Imamizu, H., Ito, M., Manto, M., Marvel, C., Parker, K., Pezzulo, G., Ramnani, N., Riva, D., Schmahmann, J., Vandervert, L., Yamazaki, T., 2014. Consensus paper: The cerebellum's role in movement and cognition. Cerebellum 13, 151–177. doi:10.1007/s12311-013-0511-x

Lang, E.J., Apps, R., Bengtsson, F., Cerminara, N.L., De Zeeuw, C.I., Ebner, T.J., Heck, D.H., Jaeger, D., Jörntell, H., Kawato, M., Otis, T.S., Ozyildirim, O., Popa, L.S., Reeves, A.M.B., Schweighofer, N., Sugihara, I., Xiao, J., 2017. The Roles of the Olivocerebellar Pathway in Motor Learning and Motor Control. A Consensus Paper. Cerebellum 16, 230–252. doi:10.1007/s12311-016-0787-8

Lev-Ram, V., Miyakawa, H., Lasser-Ross, N., Ross, W.N., 1992. Calcium transients in cerebellar Purkinje neurons evoked by intracellular stimulation. J. Neurophysiol. 68, 1167–1177.

Loewenstein, Y., Mahon, S., Chadderton, P., Kitamura, K., Sompolinsky, H., Yarom, Y., Hausser, M., 2005. Bistability of cerebellar Purkinje cells modulated by sensory stimulation. Nat. Neurosci. 8, 202–211. doi:10.1038/nn1393

Longair, M.H., Baker, D.A., Armstrong, J.D., 2011. Simple neurite tracer: Open source software for reconstruction, visualization and analysis of neuronal processes. Bioinformatics 27, 2453–2454. doi:10.1093/bioinformatics/btr390

Marr, D., 1969. A theory of cerebellar cortex. J. Physiol. 202, 437–470. doi:10.1113/jphysiol.1969.sp008820

Masino, M. a, Fetcho, J.R., 2005. Fictive swimming motor patterns in wild type and mutant larval zebrafish. J. Neurophysiol. 93, 3177–88. doi:10.1152/jn.01248.2004

Matsui, H., Namikawa, K., Babaryka, A., Köster, R.W., 2014. Functional regionalization of the teleost cerebellum analyzed in vivo. Proceedings of the National Academy of Sciences of the United States of America. doi:10.1073/pnas.1403105111

Mathews, P.J., Lee, K.H., Peng, Z., Houser, C.R., Otis, T.S., 2012. Effects of Climbing Fiber Driven Inhibition on Purkinje Neuron Spiking. J. Neurosci. 32, 17988–17997. doi:10.1523/JNEUROSCI.3916-12.2012

Medina, J.F., Lisberger, S.G., 2007. Variation, Signal, and Noise in Cerebellar Sensory-Motor Processing for Smooth-Pursuit Eye Movements. J. Neurosci. 27, 6832–6842. doi:10.1523/JNEUROSCI.1323-07.2007

Miall, R.C., Weir, D.J., Wolpert, D.M., Stein, J.F., 1993. Is the cerebellum a smith predictor? J. Mot. Behav. 25, 203–216. doi:10.1080/00222895.1993.9942050

Nagel, G., Brauner, M., Liewald, J.F., Adeishvili, N., Bamberg, E., Gottschalk, A., 2005. Light activation of Channelrhodopsin-2 in excitable cells of caenorhabditis elegans triggers rapid behavioral responses. Curr. Biol. 15, 2279–2284. doi:10.1016/j.cub.2005.11.032

Ohmae, S., Medina, J.F., 2015. Climbing fibers encode a temporal-difference prediction error during cerebellar learning in mice. Nat. Neurosci. 18. doi:10.1038/nn.4167

Ozden, I., Dombeck, D.A., Hoogland, T.M., Tank, D.W., Wang, S.S.-H., 2012. Widespread State-Dependent Shifts in Cerebellar Activity in Locomoting Mice. PLoS One 7, e42650. doi:10.1371/journal.pone.0042650

Ozol, K., Hayden, J.M., Oberdick, J., Hawkes, R., 1999. Transverse zones in the vermis of the mouse cerebellum. J. Comp. Neurol. 412, 95–111. doi:10.1002/(SICI)1096-9861(19990913)412:1<95::AID-CNE7>3.0.CO;2-Y

Palay, S.L., Chan-Palay, V., 1974. Cerebellar cortex: cytology and organization. Springer-Verlag, New York. doi: 10.1007/978-3-642-65581-4

Pedregosa, F., Varoquaux, G., Gramfort, A., Michel, V., Thirion, B., Grisel, O., Blondel, M., Prettenhofer, P., Weiss, R., Dubourg, V., Vanderplas, J., Passos, A., Cournapeau, D., Brucher, M., Perrot, M., Duchesnay, É., 2012. Scikit-learn: Machine Learning in Python. J. Mach. Learn. Res. 12, 2825–2830. doi:10.1007/s13398-014-0173-7.2

Pivetta, C., Esposito, M.S., Sigrist, M., Arber, S., 2014. Motor-circuit communication matrix from spinal cord to brainstem neurons revealed by developmental origin. Cell 156, 537–48. doi:10.1016/j.cell.2013.12.014

Popa, L.S., Streng, M.L., Ebner, T.J., 2018. Purkinje Cell Representations of Behavior: Diary of a Busy Neuron. Neuroscientist. doi:10.1177/1073858418785628

Porrill, J., Dean, P., Stone, J. V., 2004. Recurrent cerebellar architecture solves the motor-error problem. Proc. R. Soc. B Biol. Sci. 271, 789–796. doi:10.1098/rspb.2003.2658

Porrill, J., Dean, P., Anderson, S.R., 2013. Adaptive filters and internal models: Multilevel description of cerebellar function. Neural Networks 47, 134–149. doi:10.1016/j.neunet.2012.12.005

Portugues, R., Feierstein, C.E., Engert, F., Orger, M.B., 2014. Whole-brain activity maps reveal stereotyped, distributed networks for visuomotor behavior. Neuron 81, 1328–1343. doi:10.1016/j.neuron.2014.01.019

Powell, K., Mathy, A., Duguid, I., Häusser, M., 2015. Synaptic representation of locomotion in single cerebellar granule cells. Elife 4, 1–18. doi:10.7554/eLife.07290

Raman, I.M., Bean, B.P., 1997. Resurgent sodium current and action potential formation in dissociated cerebellar Purkinje neurons. J. Neurosci. 17, 4517–26.

Ramirez, J.E., Stell, B.M., 2016. Calcium Imaging Reveals Coordinated Simple Spike Pauses in Populations of Cerebellar Purkinje Cells. Cell Rep. 17, 3125–3132. doi:10.1016/j.celrep.2016.11.075

Raymond, J.L., Medina, J.F., 2018. Computational Principles of Supervised Learning in the Cerebellum. Annu. Rev. Neurosci. 41, 233–253. doi:10.1146/annurev-neuro-080317-061948

Requarth, T., Kaifosh, P., Sawtell, N.B., 2014. A Role for Mixed Corollary Discharge and Proprioceptive Signals in Predicting the Sensory Consequences of Movements. J. Neurosci. 34, 16103–16116. doi:10.1523/JNEUROSCI.2751-14.2014

Rohlfing, T., Maurer, C.R., 2003. Nonrigid image registration in shared-memory multiprocessor environments with application to brains, breasts, and bees. IEEE Trans. Inf. Technol. Biomed. 7, 16–25.

Sauerbrei, B.A., Lubenov, E.V., Siapas, A.G., 2015. Structured Variability in Purkinje Cell Activity during Locomotion. Neuron 87, 840–852. doi:10.1016/j.neuron.2015.08.003

Scalise, K., Shimizu, T., Hibi, M., Sawtell, N.B., 2016. Responses of cerebellar Purkinje cells during fictive optomotor behavior in larval zebrafish. J. Neurophysiol. 116, 2067–2080. doi:10.1152/jn.00042.2016

Sengupta, M., Thirumalai, V., 2015. AMPA receptor mediated synaptic excitation drives state-dependent bursting in Purkinje neurons of zebrafish larvae. Elife 4, 1–21. doi:10.7554/eLife.09158

Severi, K.E., Portugues, R., Marques, J.C., O'Malley, D.M., Orger, M.B., Engert, F., 2014. Neural Control and Modulation of Swimming Speed in the Larval Zebrafish. Neuron 83, 692–707. doi:10.1016/j.neuron.2014.06.032

Simpson, J.I., Wylie, D.R., De Zeeuw, C.I., 1996. On climbing fiber signals and their consequence (s). Behav. Brain Sci. 19, 384–398.

Simpson, J.I., Alley, K.E., 1974. Visual climbing fiber input to rabbit vestibulo-cerebellum: a source of direction-specific information. Brain Res. 82, 302–308. doi:10.1016/0006-8993(74)90610-6

Soetedjo, R., Fuchs, A.F., 2006. Complex Spike Activity of Purkinje Cells in the Oculomotor Vermis during Behavioral Adaptation of Monkey Saccades. J. Neurosci. 26, 7741–7755. doi:10.1523/JNEUROSCI.4658-05.2006

Steinmetz, J.E., Logan, C.G., Rosen, D.J., Thompson, J.K., Lavond, D.G., Thompson, R.F., 1987. Initial localization of the acoustic conditioned stimulus projection system to the cerebellum

essential for classical eyelid conditioning. Proc. Natl. Acad. Sci. U. S. A. 84, 3531–5. doi:10.1073/pnas.84.10.3531

Steinmetz, J.E., Rosen, D.J., Chapman, P.F., Lavond, D.G., Thompson, R.F., 1986. Classical conditioning of the rabbit eyelid response with a mossy-fiber stimulation CS: I. Pontine nuclei and middle cerebellar peduncle stimulation. Behav. Neurosci. doi:10.1037/0735-7044.100.6.878

Stoodley, C.J., Valera, E.M., Schmahmann, J.D., 2012. Functional topography of the cerebellum for motor and cognitive tasks: An fMRI study. Neuroimage 59, 1560–1570. doi:10.1016/j.neuroimage.2011.08.065

Streng, M.L., Popa, L.S., Ebner, T.J., 2018. Complex Spike Wars: a New Hope. Cerebellum 1–12. doi:10.1007/s12311-018-0960-3

Suvrathan, A., Payne, H.L., Raymond, J.L., 2016. Timing Rules for Synaptic Plasticity Matched to Behavioral Function. Neuron 92, 959–967. doi:10.1016/j.neuron.2016.10.022

Takeuchi, M., Matsuda, K., Yamaguchi, S., Asakawa, K., Miyasaka, N., Lal, P., Yoshihara, Y., Koga, A., Kawakami, K., Shimizu, T., Hibi, M., 2015. Establishment of Gal4 transgenic zebrafish lines for analysis of development of cerebellar neural circuitry. Dev. Biol. 397, 1–17. doi:10.1016/j.ydbio.2014.09.030

Takeuchi, M., Yamaguchi, S., Sakakibara, Y., Hayashi, T., Matsuda, K., Hara, Y., Tanegashima, C., Shimizu, T., Kuraku, S., Hibi, M., 2017. Gene expression profiling of granule cells and Purkinje cells in the zebrafish cerebellum. J. Comp. Neurol. 525, 1558–1585. doi:10.1002/cne.24114

Temizer, I., Donovan, J.C., Baier, H., Semmelhack, J.L., 2015. A Visual Pathway for Looming-Evoked Escape in Larval Zebrafish. Curr. Biol. 25, 1823–1834. doi:10.1016/j.cub.2015.06.002

ten Brinke, M.M., Boele, H., Spanke, J.K., Ijpelaar, A.C.H.G., Zeeuw, C.I. De, Brinke, M.M., Boele, H., Spanke, J.K., Potters, J., Kornysheva, K., Wulff, P., 2015. Evolving Models of Pavlovian Conditioning : Cerebellar Cortical Dynamics in Awake Behaving Mice. Cell Reports 13, 1977–1988. doi:10.1016/j.celrep.2015.10.057

Thiele, T.R., Donovan, J.C., Baier, H., 2014. Descending Control of Swim Posture by a Midbrain Nucleus in Zebrafish. Neuron 83, 679–691. doi:10.1016/j.neuron.2014.04.018

van Beugen, B.J., Gao, Z., Boele, H.-J., Hoebeek, F., De Zeeuw, C.I., 2013. High frequency burst firing of granule cells ensures transmission at the parallel fiber to purkinje cell synapse at the cost of temporal coding. Front. Neural Circuits 7, 95. doi:10.3389/fncir.2013.00095

van der Walt, S., Schönberger, J.L., Nunez-Iglesias, J., Boulogne, F., Warner, J.D., Yager, N., Gouillart, E., Yu, T., 2014. scikit-image: image processing in Python. PeerJ 2, e453. doi:10.7717/peerj.453

Wagner, M.J., Kim, T.H., Savall, J., Schnitzer, M.J., Luo, L., 2017. Cerebellar granule cells encode the expectation of reward. Nature 544, 96–100. doi:10.1038/nature21726

Witter, L., De Zeeuw, C.I., 2015. Regional functionality of the cerebellum. Curr. Opin. Neurobiol. 33, 150–155. doi:10.1016/j.conb.2015.03.017

Wolpert, D.M., Miall, R.C., Kawato, M., 1998. Internal models in the cerebellum. Trends Cogn. Sci. 2, 338–347. doi:10.1016/S1364-6613(98)01221-2

Wylie, D.R., Frost, B.J., 1991. Purkinje cells in the vestibulocerebellum of the pigeon respond best to either translational or rotational wholefield visual motion. Exp. Brain Res. 86, 229–232. doi:10.1007/BF00231059

Xiao, J., Cerminara, N.L., Kotsurovskyy, Y., Aoki, H., Burroughs, A., Wise, A.K., Luo, Y., Marshall, S.P., Sugihara, I., Apps, R., Lang, E.J., 2014. Systematic regional variations in Purkinje cell spiking patterns. PLoS One 9. doi:10.1371/journal.pone.0105633

Zhou, H., Lin, Z., Voges, K., Ju, C., Gao, Z., Bosman, L.W.J., Ruigrok, T.J., Hoebeek, F.E., De Zeeuw, C.I., Schonewille, M., 2014. Cerebellar modules operate at different frequencies. Elife 2014, 1–18. doi:10.7554/eLife.02536

Zhou, H., Voges, K., Lin, Z., Ju, C., Schonewille, M., 2015. Differential Purkinje cell simple spike activity and pausing behavior related to cerebellar modules. J. Neurophysiol. 113, 2524–2536. doi:10.1152/jn.00925.2014

MULTIMEDIA FILES

Movie S1. Z-projection map of GCaMP6s responses (max dF/F) in Purkinje cells to visual stimuli. See Figure 1.

SUPPLEMENTAL FIGURES AND LEGENDS

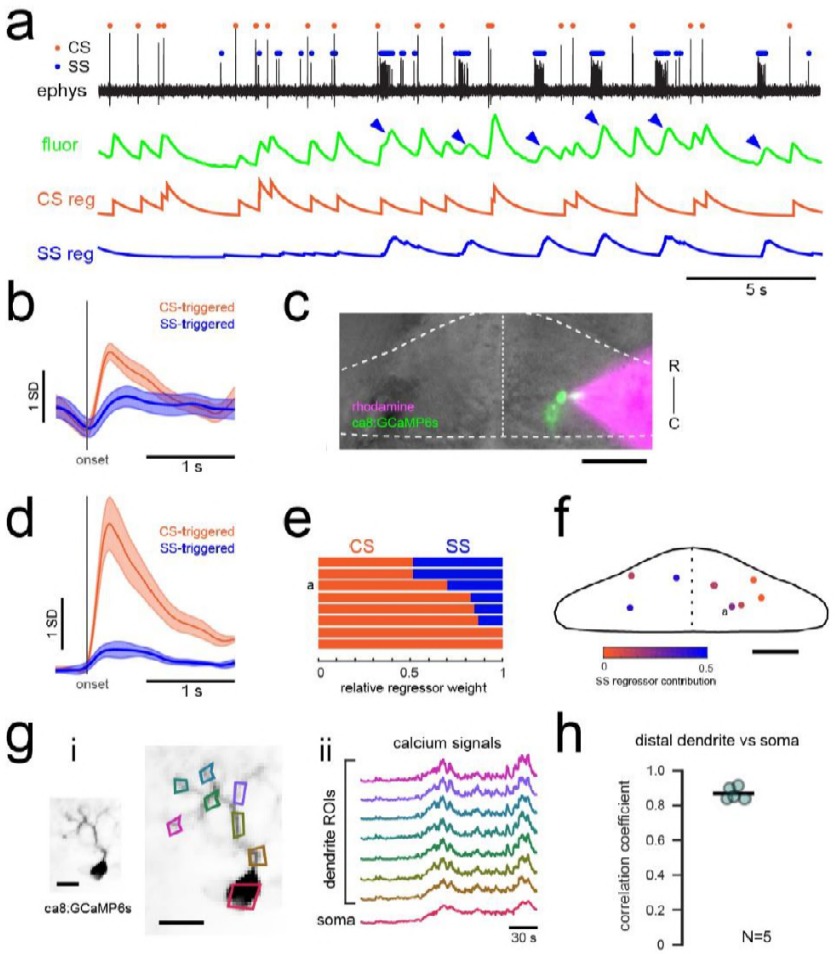

Figure S1. Related to Figure 1. Calcium signals report complex spikes reliably but can also report simple spike bursts

a) Example cell-attached electrophysiological recording (ephys, black trace) and simultaneously recorded fluorescence trace (green) from a Purkinje cell expressing GCaMP6s under the Purkinje cell-specific ca8 enhancer. All complex spikes (orange dots) are accompanied by an increase in fluorescence as shown as a deflection in the fluorescence trace that accounts for every peak in the complex spike regressor (orange trace, spike rate convolved with GCaMP kernel). In contrast, only high frequency bursts of simple spikes (blue dots) influence the fluorescence signal (indicated by blue arrowheads). b) The mean spike-triggered fluorescence signal and standard deviation is plotted for the example cell from a) for complex and simple spike bursts (N=25 each). c) A composite epifluorescent image showing a bright field bird's eye image of the cerebellum together with single-cell GCaMP expression in the Purkinje cell from the previous panels and the rhodamine-filled electrode contacting this cell. The outline and midline of the cerebellum is indicated by the dashed white line. Scalebar = 50 microns. d) The mean spike-triggered fluorescence signal and standard error is plotted for eight cells (N=6 fish) for complex and simple spike bursts. e) The relative contribution of the complex spike (CS) and simple spike (SS) regressors (spike rates convolved with the GCaMP kernel) to the fluorescence signal in each cell as determined by least squares regression (see Methods) across the

eight cells. The example cell from a) is indicated. f) The location of all example cells, color-coded by relative SS regressor contribution. g) Overview of i) the morphology of a singly-labelled Purkinje cell and the subcellular regions of interest (ROIs) with ii) corresponding calcium signals obtained from high resolution two-photon imaging (see Methods). Scale bars = 20 microns. h) Quantification of the correlation coefficient between the calcium signal from the most distal dendritic segment and the soma. N=5 cells from 3 fish.

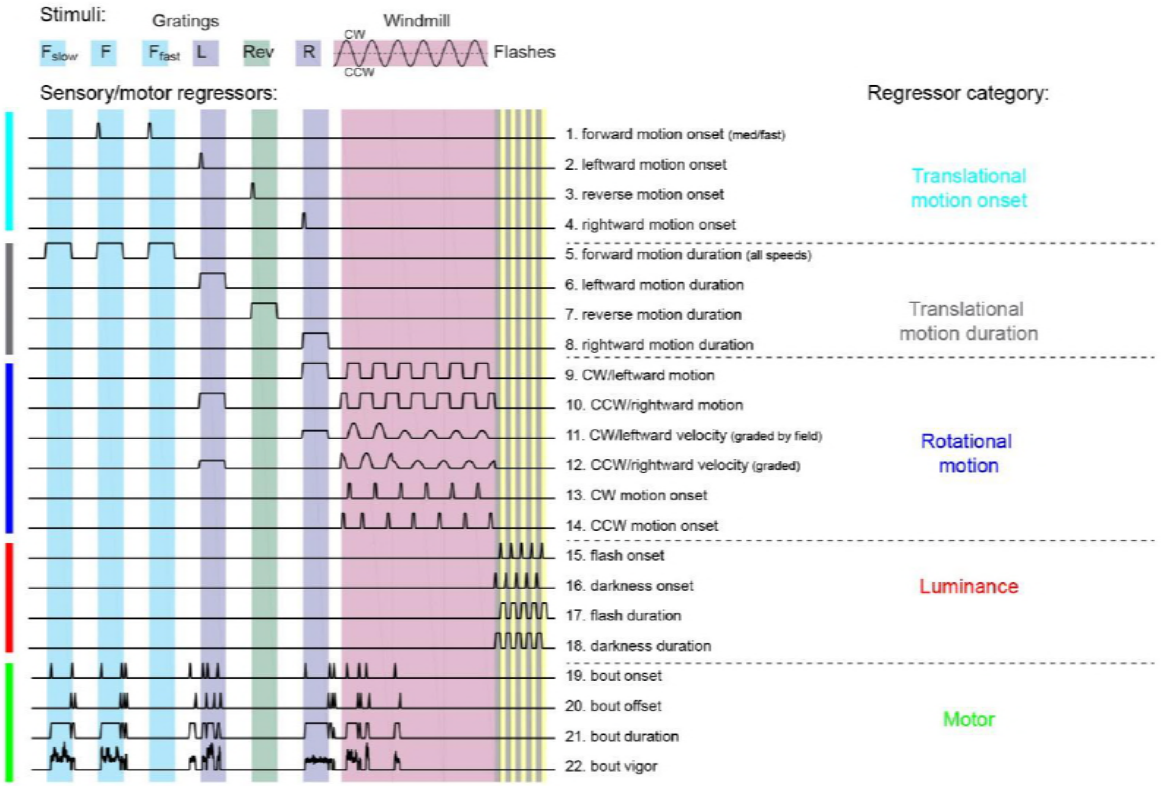

Figure S2. Related to Figure 2. Sensory and motor regressors used for multilinear least-squares regression

Top, description of stimuli used in the electrophysiological experiments (see methods and Figure 2 for details). Gratings speeds are 10mm/s with additional slow (F_{slow}, 3 mm/s) and fast (F_{fast}, 30mm/s) speeds for forward grating stimuli. The windmill stimulus rotated at sinusoidal velocities in the clockwise (CW) and counter-clockwise (CCW) directions with a frequency of 0.2 Hz. Six total periods were shown, with the first two periods being whole-field windmills, the second two periods restricted to the left visual field only, and the final two periods restricted to the right visual field only. Below, the complete set of regressors used in analysis of electrophysiological data. Individual regressors fall into one of five categories (four sensory or one motor), as indicated by the colored bars at left and the category names at the right. Regressors 19-21 are calculated for each cell based on the motor activity in that trial, therefore a representative example from one trial in the dataset is shown here.

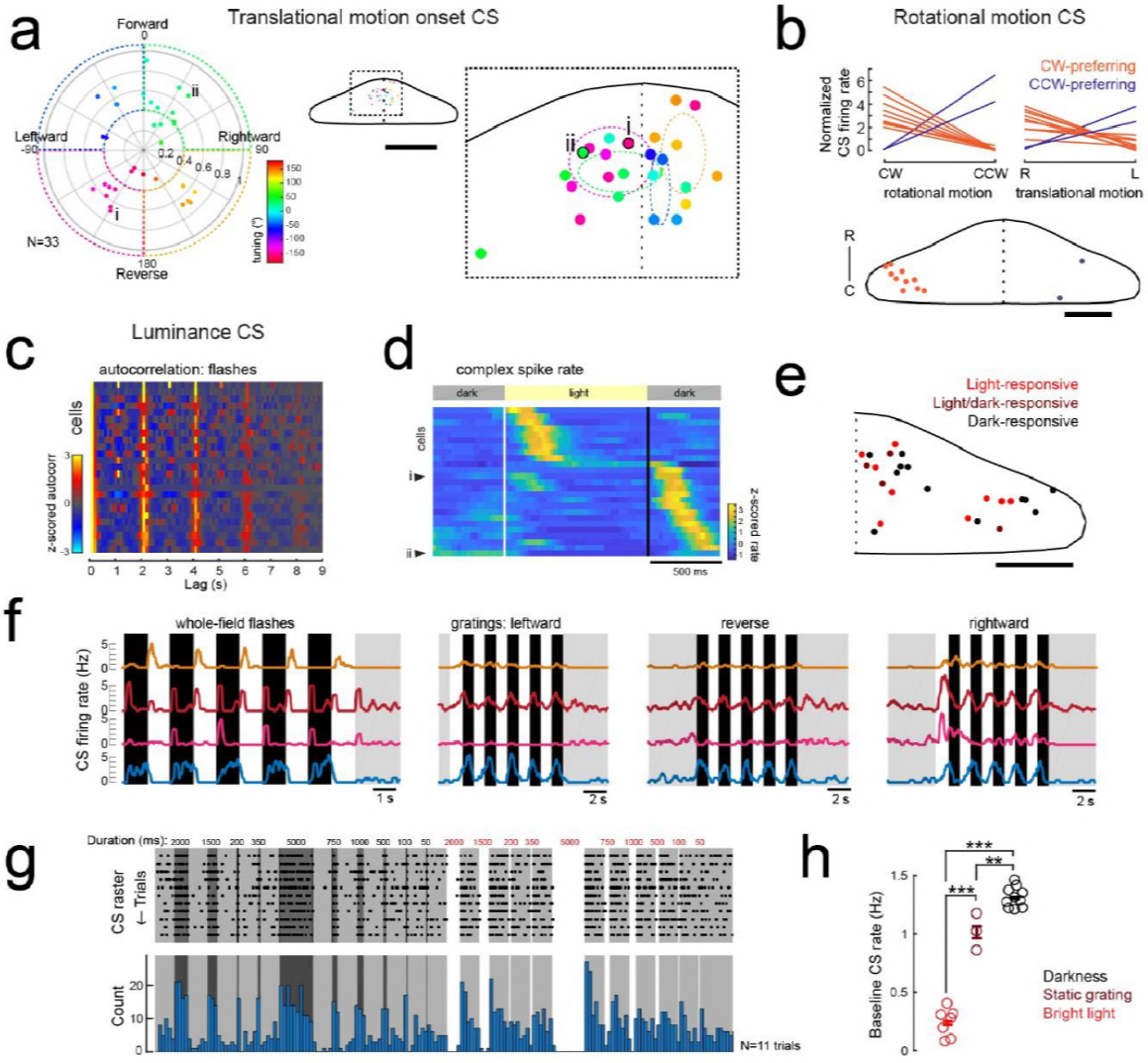

Figure S3. Related to Figure 3. Complex spike responses encode specific aspects of visual features

a) Left, polar plot of all Purkinje cells with a significant contribution to complex spike activity from the onset of translational motion in a given direction (N=33/61 cells). The tuning of the cells is indicated by the polar coordinates as well as the marker color, with 0° indicating forward motion. The distance from the center indicates the direction selectivity index of the cell (see Methods). Dashed areas indicate the four quadrants used for binning. Right, the location of all cells with this complex spike phenotype within the quadrants are plotted onto a flattened bird's eye view of the cerebellum (example cells I and ii from Figure 3a are indicated and outlined in black). The overview shows the zoomed-in region of the rostromedial cerebellum. Colors indicate tuning preference as shown at left. Dotted ellipses indicate the boundary for the mean location and SEM for each group of similarly tuned cells. Scale bar = 100 microns for overview, 500 microns for cropped zoom. b) Upper plots, the mean complex spike firing rate (normalized to baseline, dotted black line) of all Purkinje cells with significant coefficient weights for rotational motion regressors (N=11) is shown for both the duration of rotational motion in a given direction (left plot) and the duration of leftward and rightward translational motion (right plot). Two distinct groups are clearly seen that prefer either clockwise and rightward motion (orange lines) or counter-clockwise and leftward motion (blue lines). Lower panel, the location of all

cells with this complex spike phenotype are plotted onto a flattened bird's eye view of the cerebellum. Colors indicate rotational motion preference. Scale bar = 50 microns. c) Left, all luminance-responsive cells as determined by significant autocorrelation values for whole-field flashes for the 2 second lag (N=25/61) are plotted in a heat map sorted by maximum autocorrelation value for the 2 s lag. Cells are ordered by peak autocorrelation at 2s. d) Z-scored complex spike firing rates for all luminance-responsive Purkinje cells averaged across flash repetitions and sorted by the timing of their peak firing rate are shown as a heatmap. Black lines mark the transition from dark to light and back again as indicated by the grey bars above. Example cells from Figure 3c are indicated. N=25 cells. e) The location of all cells with a luminance complex spike phenotype are plotted onto a flattened bird's eye view of the cerebellum with all coordinates flipped to the right half of the cerebellum. Colors indicate the preference for light or dark flashes (or both). Scale bar = 50 microns.f) Four example Purkinje cell mean complex spike firing rates in response to whole-field flashes (left) and three directions of moving gratings (right) show different responses to global versus local luminance changes. g) Additional recordings from a luminance-responsive Purkinje cell (see Figure 3cii) during the presentation of whole-field black (here shown as dark grey) and white flashes of various durations (50 - 5000 ms) from a baseline intermediate luminance (light grey). Upper panel, raster plot of complex spikes across trials (N=11). Lower panel, complex spike count histogram. This cell produces has a clear sustained increase in complex spike activity during darkness whereas complex spike activity is nearly absent during bright flashes. h) Quantification of the baseline complex spike firing rate of the cell in g) in the absence of changing visual stimuli for three different whole-field luminance levels. Three asterisks indicate $p<0.001$ and two indicate $p<0.01$ as calculated by one-way ANOVA with Bonferroni post hoc correction.

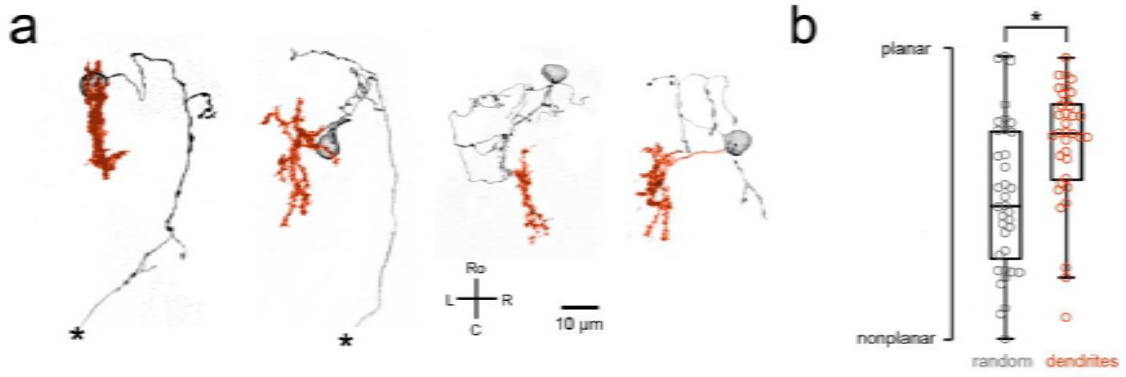

Figure S4. Related to Figure 3. Purkinje cell dendrites show a mostly planar morphology

1570

a) Four example Purkinje cell morphologies obtained by single-cell labeling (see Methods) are shown with their soma and axon in black and dendrites in orange. Asterisks indicate a truncated axon. b) Quantification of dendritic morphology as measured by determining the principal axes (see Methods) shows that dendrites are significantly more planar than chance ($p<0.01$, Wilcoxon signed rank test).

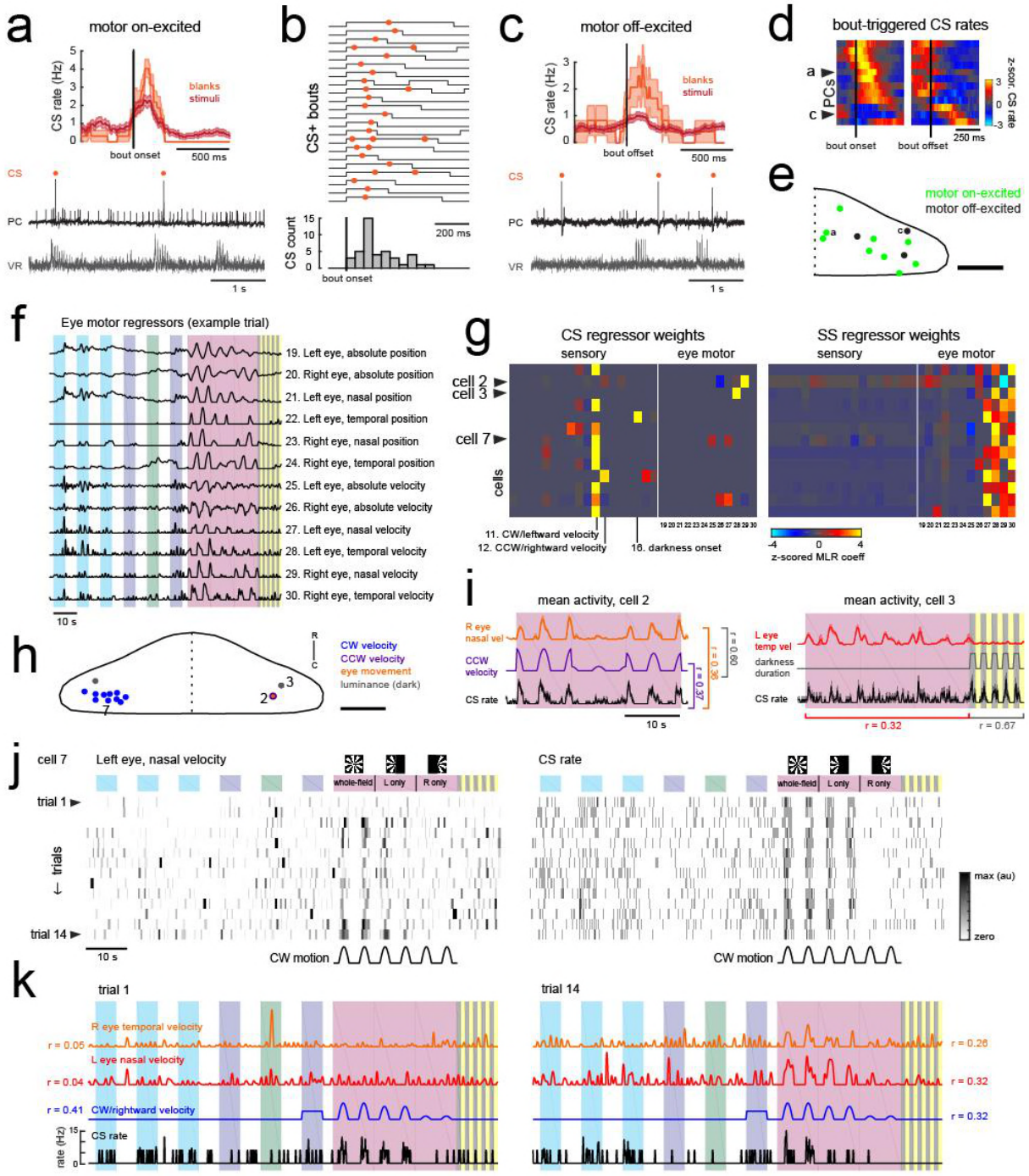

Figure S5. Related to Figure 3. Motor-related complex spikes are rare

a) Upper plot, the mean bout-triggered complex spike rate with shaded SEM for this cell for all swim bouts during the blank recordings (no stimuli presented, orange trace) and during trials with visual stimuli (red trace). N = 16 bouts (blanks), 76 bouts (stimuli). Lower traces, example excerpt from a blank recording from this Purkinje cell (PC, black trace) with simultaneous ventral root recording (VR, gray trace, shown as a moving standard deviation). Complex spikes are indicated by orange dots above the trace. b) Upper traces, a subset of bouts are plotted aligned to bout onset for swim episodes during which a complex spike occurred

(orange dot). Below, a normalized histogram for all CS+ bouts in this recording show that the majority of the complex spikes are triggered in the period 100-150 ms following bout onset (N=34/76 CS+ bouts). c) Upper plot, the mean bout off-triggered complex spike rate with shaded SEM for this cell for blank and visual stimuli trials. N = 12 bouts (blanks), 468 bouts (stimuli). Lower traces, example excerpt from a blank electrophysiological recording from this cell. d) Heatmap of bout on- and off-triggered mean complex spike rates for all cells with significant motor coefficients arranged by peak CS firing rate from bout onset. The lower three rows correspond to cells that have a decrease in CS activity during bouts which increases following bout offset. The example cells from a) and c) are indicated. e) The locations of these Purkinje cells with CS activity correlated with bout onset (green) or bout offset (black) are plotted on the right lobe of a reference cerebellum (some coordinates were flipped from left to right). The example cells from a) and c) are indicated. Scale bar = 50 microns. f) The 12 eye motor regressors used for multilinear least squares regression (MLR) of electrophysiological data with eye movements in the semi-paralyzed zebrafish (see Methods for details; see Figure S2 for the description of sensory regressors). All eye motor regressors are calculated for each cell based on the motor activity of each eye (tracked independently) in that trial. A representative set of regressors computed from eye movement in one trial in the dataset is shown here. g) Heatmap of all 30 regressor coefficient weights (18 sensory and 12 eye motor) for the complex spike (left) and simple spike (right) firing rates of 13 cells (N=11 fish). The sensory regressors with the largest coefficient weights for complex spike rates are indicated. For complex spike phenotypes, 11/13 Purkinje cells have a stronger "sensory" phenotype, whereas 13/13 Purkinje cell have a simple spike "motor" phenotype. The two remaining Purkinje cells with a motor complex spike phenotype are indicated as ci and cii (arrowheads). h) Location of all cells, color-coded for complex spike phenotype as determined by MLR and additional analyses (see subsequent panels). Scale bar = 50 microns. i) Left, mean activity and SEM for the complex spike rate and best eye movement regressor excerpted from the rotational stimulus portion of the experiment for Purkinje cell 2 as indicated in g) and classified as having a motor complex spike phenotype. The single correlation coefficient between the best motor and sensory regressors across trials are very high (r = 0.60 across the full trial). Right, mean activity and SEM for the complex spike rate and best eye movement regressor excerpted from the rotational stimulus and flash portion of the experiment for Purkinje cell 3 as indicated in b) and the only other cell classified as having a “motor” complex spike phenotype. The single correlation coefficient values for the complex spike rate with the indicated regressors across trials for just the rotational stimulus period or just the luminance period are shown. j) Heatmap of eye movement (left eye, nasal) and complex spike rates across all trials of an experiment for a representative Purkinje cell in the left caudolateral cerebellum (cell 7 as indicated in g,h). Note the variability of the eye movement across trials (left) compared to the complex spike rate (right). Clockwise velocity is indicated for reference. k) The best motor regressors for each eye and the best sensory regressor are plotted against the complex spike rate of the cell in j) for the first (left) and last (right) trial of the experiment. Single correlation coefficient values are shown between each regressor and the complex spike rate for this trial. Time scale is same as for j).

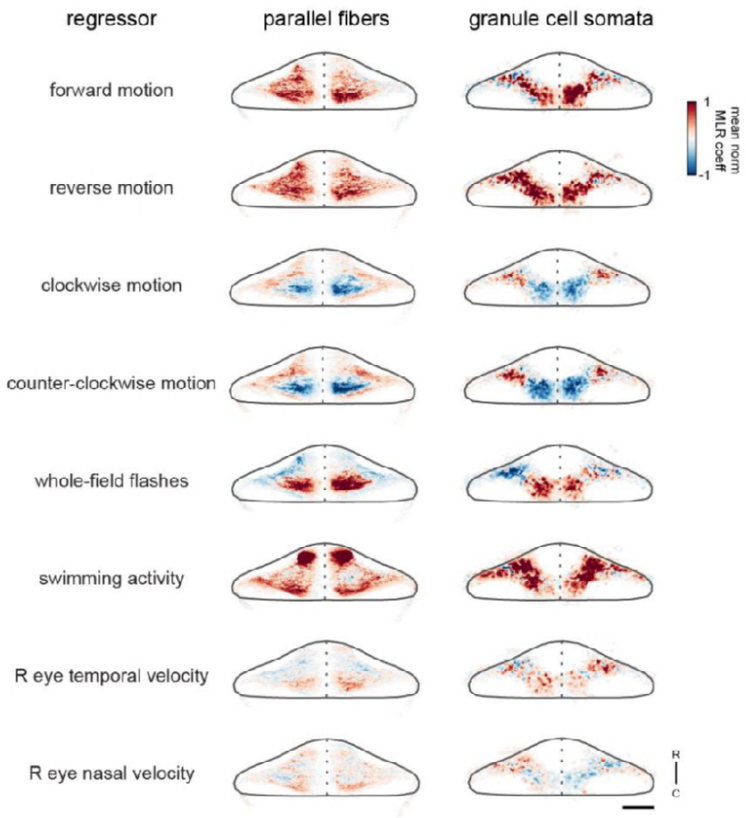

Figure S6. Related to Figure 1 and Figure 4. Swimming-related granule cell activity is distributed broadly across the cerebellum

Heatmaps of the z-projected mean voxelwise correlation coefficients of granule cell GCaMP6s signals from multilinear regression with example sensory and motor regressors averaged across 7 fish (see Methods). Scale bar = 50 microns.

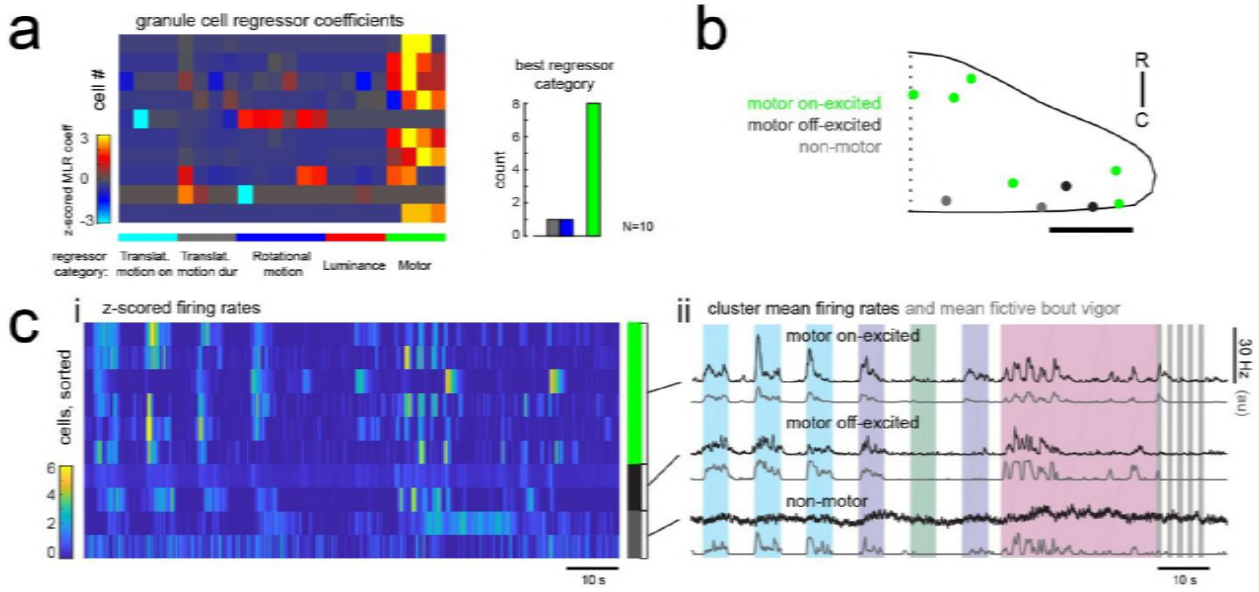

1630 **Figure S7. Related to Figure 4. Many granule cells show significant modulation of their firing rates during fictive swimming bouts**

a) Left, matrix of multilinear regressor coefficients for granule cell firing rates from all 10 cell-attached electrophysiological recordings with simultaneous fictive behavior in response to the same sensory stimuli
1635 as shown in Figure 2a. Right, histogram of cell counts for each best regressor category (as color-coded at left). b) Location of granule cells across all fish mapped onto a reference cerebellum (bird's eye view) and colored according to their motor phenotype. All coordinates are flipped onto the right hemisphere. Scale bar = 50 microns. c) Left, heatmap of z-scored mean firing rates for all granule cells sorted by decreasing motor regressor coefficient. Colored bars at right indicate cells whose firing rate is positively modulated by bout
1640 duration (green), by bout offset (black), or by neither (grey). Right, cluster mean granule cell firing rates (black) and mean fictive bout vigor (grey).